Spectral Deconvolution Algorithm (SDA)
Technical memo

Norm O'Neill, Tom Eck, Alexander Smirnov, Brent Holben

Revision history for this document

April 9, 2008 - Renamed "Version 4.0" to "Version 4.1" and added (i) a new section on "Minor modifications to the code", (ii) a new section on "Further SDA validation tests", (iii) "Special case (high Arctic data)" as a new subsection of the "Elimination of 1020 nm channel" section, (iv) a new section on "Channels employed in the SDA" and (v) Appendix A on the stochastic error model. Sections formerly under "Version 4.0" were also updated if necessary and rearranged.

April 9, 2007 - added sections on "Retrieval Errors" and "Elimination of 1020 nm channel" under "Version 4.0"

April 26, 2006 - replaced the Mean of Extrema (MOE) approach with the weighted averaging approach (new section entitled Version 4.0)

June 22, 2005 - added sections "Version 3.0" and "QA issues for Version 3.0"

Mar. 28, 2005 - document initiated with Sections "Version 1.0" and "Version 2.0"

This technical memo was written to provide more detailed technical and validation information the SDA (Spectral Deconvolution Algorithm[1]). The algorithmic development is given in (O'Neill et al., 2001b and O'Neill et al., 2003). The optical science background can be found in (O'Neill et al., 2001a) while the initial paper on the employment of spectral curvature parameters can be found in Eck et al. (1999).The SDA algorithmic development was divided into version numbers; the sections below reference these version numbers. The text is arranged in reverse chronological order (latest changes appear first).

[1] written originally as a Matlab function called tauf_tauc.m, but, for example, converted to C++ for AERONET

Version 4.1

This modified Version 4.1 section provides details on the algorithmic and code changes effected and tests performed since the introduction of Version 4.0 in the April, 9, 2007 version of the technical memo. These changes and tests (summarized in the Revision history for this document) were motivated by the goal of promoting the SDA algorithm to an AERONET level 2 product (they are, in fact, largely synonomous with the specific objective of producing a level 2 algorithm).

Minor modifications to the code

During the processing of the high Arctic data below it was recognized that an error of $\Delta\tau$ / m ($\Delta\tau$, the nominal CIMEL AOD error and m, the solar air mass) was a more realistic estimate of the input AOD error to the SDA. While this change is strictly not a property of the subroutine tauf_tauc.m it is mentioned here because the magnitude of the input error has effects when the FMF (η) is near unity. This ($\Delta\tau$ / m) is the input error which should be employed for AERONET processing.

On Mar. 19, 2008, a modified tauf_tauc.m subroutine was generated.This version corrected for a minor inconsistancy in the way $\alpha_{f,max}$(Mie theoretical) was processed[2]. This produced minor changes in α_f and τ_f (rms differences of 0.14 and 0.0018 over the whole PEARL data set described below). Neither PEARL nor the UAE[2] calculations were redone because of the minor nature of the changes (although checks were made to ensure that the differences were negligible). Comparisons with the definitive Mongu case of Figure 7 showed differences which differed by only one or two digits in the last digit of the means shown in Figure 7.

On April 1, 2008 a modified version of the error model in tauf_tauc.m was generated. This version corrected some errors in the theoretical formulation (the partial derivatives given in O'Neill et al., (2003)) and the manner in which the error due to the assumed dependence of α'_f vs α_f was incorporated. These corrected formulations are now included in Appendix A below (an Appendix which supercedes Appendix A of O'Neill et al., (2003)). The rms differences relative to the tauf_tauc.m version discussed immediately above were 0.037 and 0.0010 over the whole PEARL data set. Mongu comparisons showed differences of less than one digit in the rms values shown in Figure 7 with a moderate increase of the coefficient of determination from 0.429 to 0.491.

Further SDA validation tests

The tests in this section were performed without the elimination of the 1020 nm channel. In part this was because some of the work was started before the decision was taken to eliminate this channel in the AERONET processing chain but as well because it was found, in the case of the high Arctic data that the inclusion of 1020 nm results produced more physically realistic results. A discussion of this particular case is given in the section explicitly dedicated to the elimination of the 1020 nm channel.

High Arctic data

[2] The major effect of this inconsistancy were occasionnal jumps in α_f when α_f was excessively low

It was demonstrated in O'Neill et al. (2008b) that the SDA algorithm continued to produce physically consistent fine and coarse mode optical depth results (in comparison with backscatter (β) and depolarization-ratio (δ) profiles from a high spectral resolution lidar[3]) at the Eureka, Nunavut atmospheric observatory (80.05° N latitude). The red τ_f curve of Figure 1 shows qualitative correlation with the β plume (2nd row of graphs) at around 9 km altitude while the corresponding δ values in the third row of graphs appear to be systematically small amidst a clutter of noise. Extreme excursions in τ_c (blue curve) correspond to strong β signals on July 21 and 24 which, in turn, correspond to elevated (reddish) δ values; the strong τ_c variation and the high δ values indicate that these events are most likely due to thin cloud.

The very small AODs typical of this site made SDA retrievals more sensitive to measurement errors and algorithmic uncertainties. This fact along with the availability of synchronized AHSRL profiles, the continuous (24 hour) sunlight coupled with the use of a high frequency (3-minute) CIMEL mode ensured that this data would make an ideal test-bed for the validation of the SDA in general and the analysis of the effect of eliminating the 1020 nm channel in particular (see the following section).

This study was really the first comprehensive validation of τ_f and τ_c using lidar data (both the extensive information available from the backscatter coefficient and the intensive information available from the depolarization ratio). It re-confirmed that τ_c was a robust indicator of thin-cloud events (large backscatter coefficient and large depolarization ratio) and that τ_f was consistently indicative of fine mode events (weak backscatter coefficient and small depolarization ratio).

[3] the AHSRL (Arctic High Spectral Resolution Lidar) of Ed Eloranta (University of Wisconsin)

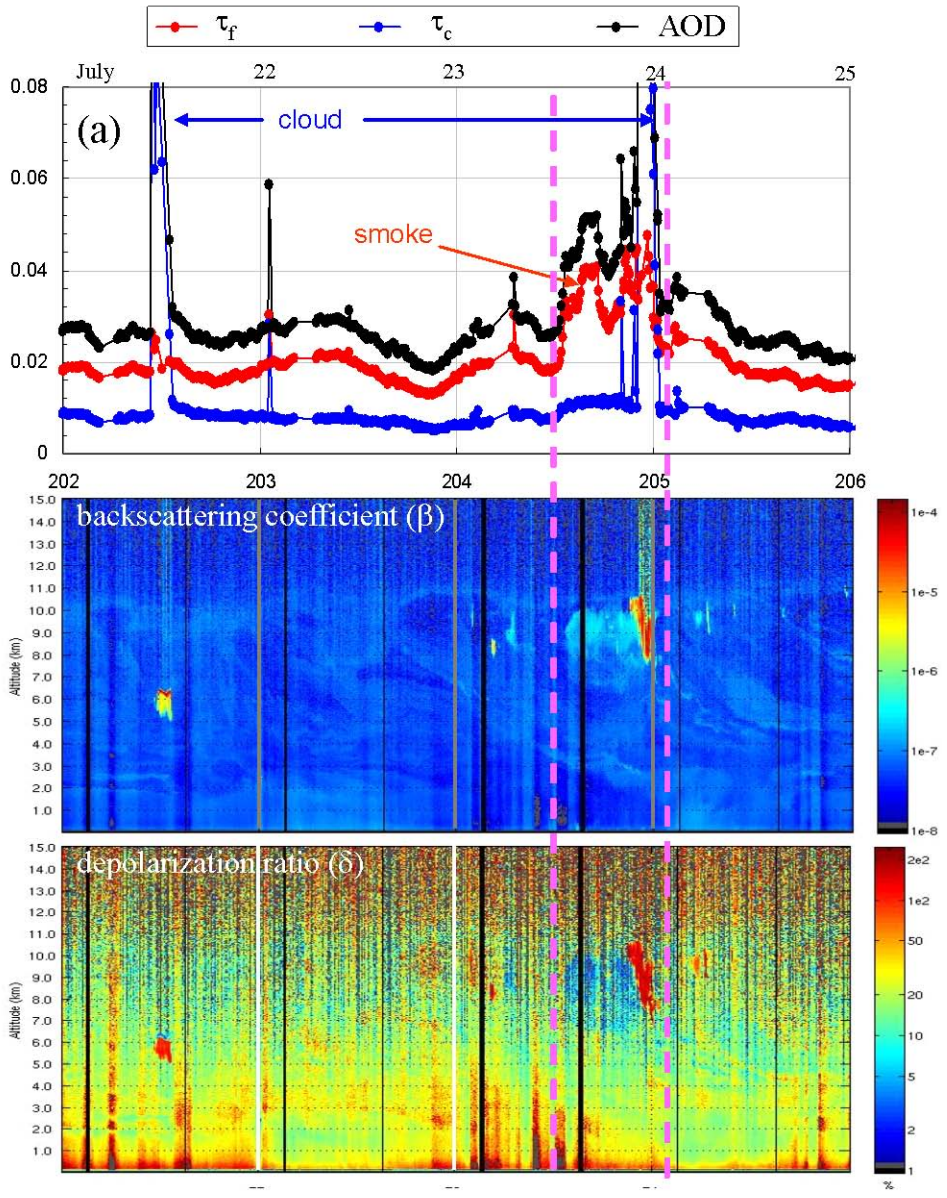

Figure 1 - SDA and AHRSL results from Eureka

Validation relative to the AERONET inversion

Some validation work relative to AERONET inversions (Dubovik et al., 2000) was performed in O'Neill et al. (2003). In that paper it was hypothesized that a major part of the differences obtained between SDA and AERONET estimates of τ_c and τ_f was due to the optical versus mechanical differences between the two approaches[4]. If this is the case then one would suppose that the normalized optical difference between the two methods would be a strong function of the mechanical cutoff fraction;

$$\frac{\Delta\tau_c}{\tau_c} = \frac{\tau_c - \tau_c'}{\tau_c} = \frac{S_c - S_c'}{S_c} = f\left(\frac{\Delta S_c}{S_c}\right) \qquad (1)$$

where S_c refers to the surface size distribution ($dS_c/d\ \ln r$) integrated over all particle sizes, and where the primes are associated with parameters resulting from the coarse mode size distribution being mechanically cut off at 0.6 μm. Mie simulations with log-normal size distributions show that a fairly strong linear relationship exists between $\Delta\tau_c/\tau_c$ and $\Delta S_c/S_c$ for intermediate size particles ($0.6 <\sim r_{eff,c} <\sim 3$ μm) and thus that the normalized difference between the SDA and the AERONET retrievals (if the major discrepency between the two is the mechanical cutoff employed in computing the latter) should be similarily related to $\Delta S_c/S_c$. Figure 2 shows a sample test of this hypothesis for 2005 Hamin data (performed as part of the UAE analysis described below). $\Delta\tau_c/\tau_c$ was computed from the difference between the SDA and the AERONET retrieval while $\Delta S_c/S_c$ was computed from a log-normal fit to the coarse-mode portion of the retrieved AERONET particle size distribution. These data were filtered so that $\eta = \tau_f / \tau_a$ was < 0.4 to ensure that the fine mode was not dominant near the 0.6 μm cutoff . The correlation of Fig. 2 is moderately strong and its regression line is reasonably close to the regression line obtained from Mie calculations. This correlation of 2nd order differences confirms that the optico-physical interpretation of the differences between the two types of retrievals is reasonable.

[4] The AERONET inversion algorithm employed in this section defined the fine and coarse modes in terms of a simple cutoff at 0.6 μm (since changed in the AERONET V2 inversion algorithm but retained here since this simple definition was more suited to our validation purposes). The SDA defines fine and coarse mode contributions spectrally, a fraction of the amplitude of τ_c is due to the optical portion cut off by the AERONET mechanical approach (assuming that modal size distributions are continuous; a reasonable assumption given that different modal features are the result of different physical mechanisms). See also the section below on FMF versus SMF (the values of η returned by the SDA and the AERONET inversion results employed here).

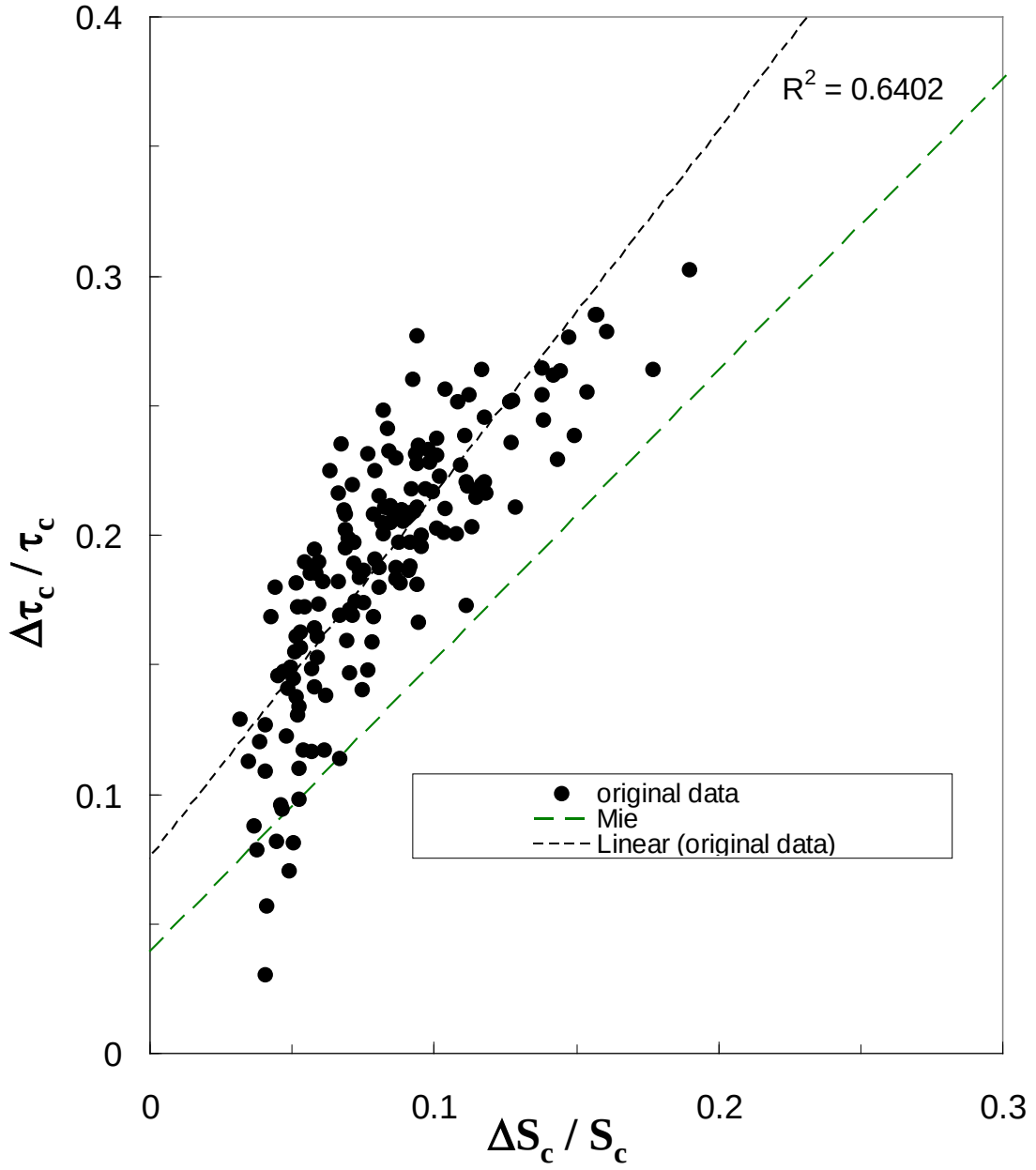

Figure 2 - Normalized difference between τ_c from the SDA and τ_c' from the AERONET inversions versus fractional cutoff of the surface particle size distribution (c.f. equation (1)).

UAE^2 experiment

Certain elements of the SDA were shown in O'Neill et al. (2008a) to be physically consistent in the face of a strong mixture of coarse and fine mode particles (dust and pollution aerosols). This analysis was carried out as part of the UAE^2 experiment (United Arab Emirates Unified Aerosol Experiment; Reid et al., 2007). It was demonstrated that τ_f and τ_c displayed an independence of behavior which would be expected for two naturally decoupled type of aerosols. A fairly strong correlation was also seen between both optical and micro-physical ground-based measurements of fine and coarse mode aerosols and the SDA retrievals. The correlation served as another confirmation of the physical consistency of the SDA and suggested a certain level of homogeniety in the vertical variation of both fine and coarse mode aerosols. An extension of the SDA (called SDA+) for analyzing spectral AOD data from those instruments with a 1.64 μm channel) was introduced in the same paper.[5]

Elimination of 1020 nm channel

General discussion

The 1020 nm channel typically displays the smallest AOD values of all the channels and is often subject to non-Mie type behavior. In spite of a temperature correction the retrieved AODs can still show temperature dependency as pointed out by at least one of us (Tom Eck). For this reason it was decided to eliminate the 1020 nm channel from the set of channels employed for the spectral deconvolution algorithm in the AERONET processing stream. This means that the set of channels previously employed for all algorithm versions {380, 440, 500, 675, 870, 1020 nm} was changed to {380, 440, 500, 675, 870 nm}.

An illustration of SDA retrieval artifacts due to a temperature sensitivity problem in the 1020 nm channel is shown in Fig. 3. One can observe an anomalous decrease in AOD(1020 nm) corresponding to a large decrease in detector temperature between 0500 and 0600. This decrease would produce a rapid decrease in the AOD spectra (rendered all the more extreme on a log-log plot) which would force the fitted polynomial to look much like a classic 2nd order (fine mode like) decrease in AOD. The result is anomalously high values of τ_f and anomalously low values of τ_c (Fig 3(c)).

[5] While no direct validation of the SDA came out of this algorithmic extension it did demonstrate the generality of the spectral curvature concept.

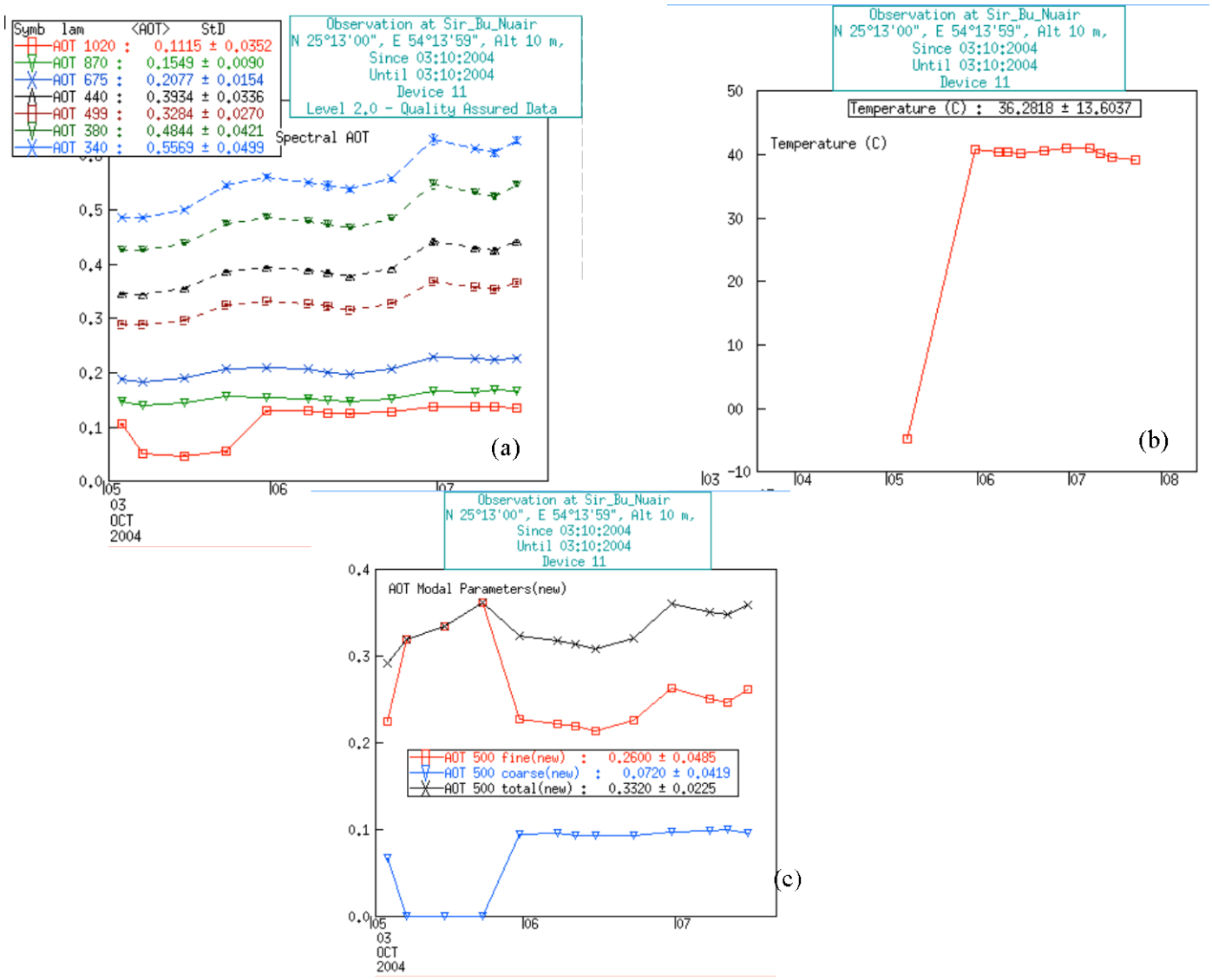

Fig. 3 - (a) AOD spectra, (b) detector temperature and (c) SDA retrievals for an obvious case of temperature artifact effects in the AOD at 1020 nm and the SDA retrievals (graphs are from the AERONET Demonstrat tool).

Table 1 shows an illustrative array of differences obtained for archived case studies between retrievals made with and without the 1020 nm channel (case studies which where not selected because of a glaring type of artifact such as seen in Fig. 3). The more extreme rms differences (notably for the Egbert retrievals of July 2002) are simply a reflection of regressed spectra varying significantly between the no-1020 and with-1020 cases[6] (as can be qualitatively appreciated in the extreme case shown in Fig. 3).

Table 1 - SDA rms retrieval differences for real and simulated data (Δx = x(no 1020) - x(with 1020).

data	N	$\Delta\tau_f$	$\Delta\tau_f/\tau_f$ (%)	$\Delta\tau_c$	$\Delta\tau_c/\tau_c$ (%)	$\Delta\eta$
Egbert, July, 2002 (V1, Level 1.0)	1004	.028	21.8	.022	60.8	.12
GSFC, 2002 (V2, Level 2.0)	6686	.010	6.4	.008	36.5	.042
Hamim, July to Dec., 2005 (Level 1.5)[7]	542	.005	2.8	.004	4.2	.012
Mie simulations (2nd order polynomial)	9	.017	15.4	.015	18.7	.020
Mie simulations (3rd order polynomial)	9	.003	1.0	.002	1.6	.004

It is important to note that the Mie differences of Table 1 are large for a second order AOD polynomial (the standard employed in the AERONET SDA algorithm) but small for a 3rd order AOD polynomial. Without the benefit of the 3rd order results the large 2nd order differences would seem illogical because the Mie curves are quite spectrally smooth; the significant reduction in differences for 3rd order results is coherent with O'Neill et al. (2001) where it was pointed out that spectral curvature relations applied to pure Mie curves required the use of higher order polynomials. How this notion translates to real data is still a debate (see the following sectioin) but for conservative reasons (to make the results less susceptable to spectral noise due to non-Mie like inter channel variation) we chose to employ a 2nd order polynomial as the AERONET standard.

[6] the inputs to the τ_f, τ_c retrieval portion of the SDA are the 500 nm values of τ_a, α and α'; these in turn are derived from a 2nd order polynomial of ln τ_a versus ln λ. The only thing that changes when the 1020 nm channel is eliminated is this polyomial and thus the input values of τ_a, α and α'.

[7] effective Level 1.5; AODs were selected only if their times matched almucanter scan times

Special case (High Arctic data)

A comparative study of SDA retrieval results was carried out with and without the 1020 nm channel in O'Neill et al. (2008b). These results were, in the first instance, consistent with the statements made in the general discussion section above; $\Delta\tau_f$ values were small and positive (rms ~ 0.006) during the summer months when temperatures were closer to the temperatures encountered during the development of the 1020 nm temperature correction algorithm and large and positive (rms ~ 0.02) during the spring when Eureka temperatures were further removed from the calibration temperatures. The reason for this behavior was obvious inasmuch as the 1020 nm AOD was abnormally large relative to the 870 nm channel, an anomaly which was especially evident when the temperature was low. Figure 4 shows the variation of $\Delta\tau_f$ with detector temperature.

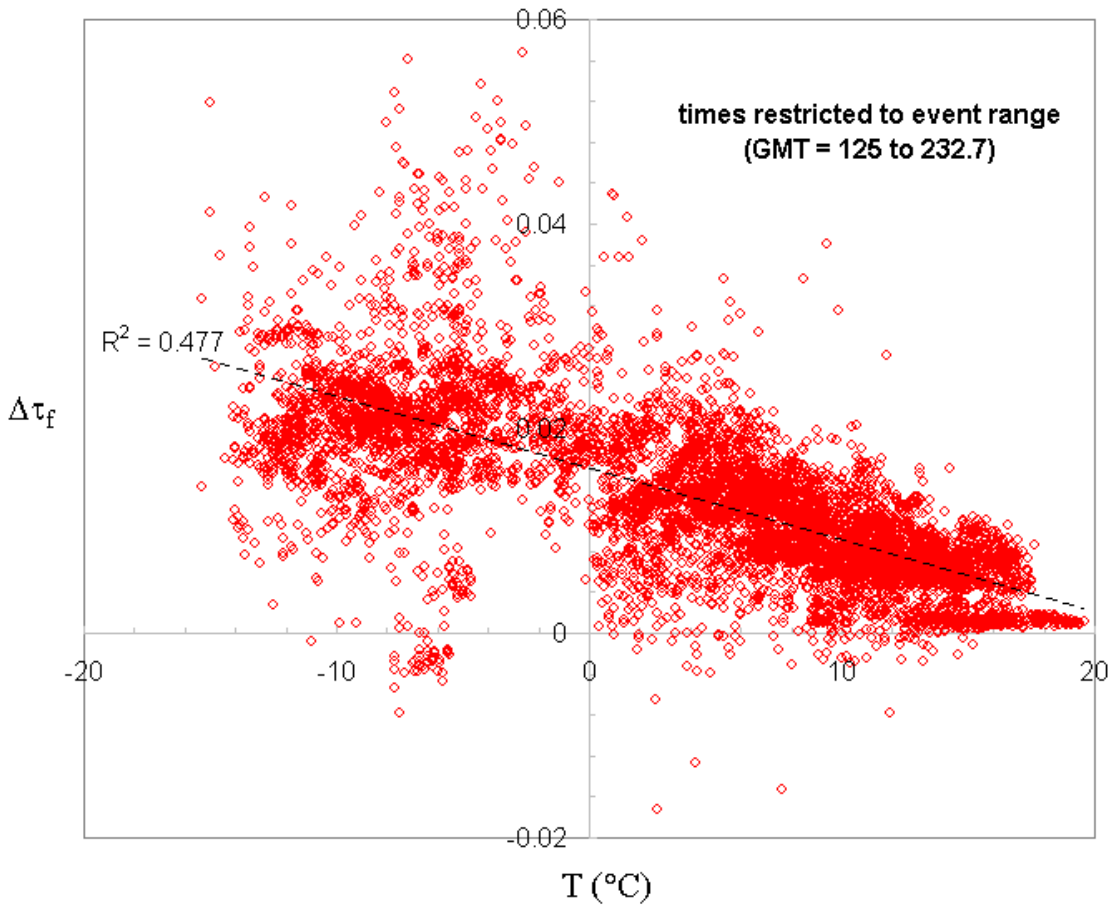

Figure 4- variation on $\Delta\tau_f$ with detector temperature (PEARL CIMEL, May 1 to Aug. 31, 2007)

The curious thing about these results however was that the no-1020 nm case produced physically unreasonable results with highly variable fine mode Angstrom exponent and unphysically small values of τ_c (negligible for the most part). Stated otherwise, τ_f and α_f were often indistinguishable from τ_a and α. The reason for this could be seen in the τ_a

spectra; the absence of the 1020 nm channel left rapidly decreasing (2nd order type) spectra which are ordinarily measured in thick atmospheres with a dominant fine mode (such as smoke). The with-1020 nm case, in spite of its temperature problems, tended to give the slow decrease in α with increasing wavelength which is expected in the presence of any kind of a reasonable coarse mode contribution (and as a consequence, reasonable values of all fine and coarse mode parameters). If one accepts the hypothesis that the coarse mode parameters were unrealistic in the no-1020 nm case then a possible explanation for this could have been that the 870 nm channel AOD was excessively low.

Reduced filter subsets; analysis of retrieval differences

The elimination of the 1020 nm channel from AERONET processing means that the standard filter set is {380, 440, 500, 675, 870} nm. Subsets of this filter set can occur for certain instruments[8] or channels in the standard set can be flagged out when a particular channel exhibits serious problems. In order to analyze the effect of subset filter sets, a series of SDA retrievals were performed on a variety of potential filter subsets. Results from a recent analysis of Horsund (Spitzbergen) data acquired in March of 2008 were employed for this purpose. This sample data set was chosen since it (like the Eureka case above) represents a high-Arctic case with low AODs and thus more difficult retrieval conditions (higher retrieval errors). It was also noted that this data set appeared to be well behaved in the sense that the spectral curvature displayed no obvious (non Mie-like anomalies). Clearly this is one sampling of the range of data sets which one might encounter across the whole AERONET ensemble of instruments; other types of reduced filter set problems will occur for other instruments but the general conclusions presented in this section will be robust enough to have universal applicabililty. We chose differences in τ_f ($\Delta\tau_f$) as an indicator of retrieval differences; because τ_a (AOD) differs little between the different reduced wavelength cases then $\Delta\tau_c$ will be strongly (and negatively) correlated with $\Delta\tau_f$ (i.e. the magnitude of $\Delta\tau_f$ will be representative of the magnitude in $\Delta\tau_c$).

Figure 5 shows the results of the analysis on the Hornsund data set applied to level 1.0 data (these results did not substantially change for level 1.5 data). One notes that the 3rd order polynomial results are, on the whole, less than the 2nd order results (6 cases out of 10). Investigation of the "Ref." (reference) vs "Stan." (AERONET standard) cases showed that the spectra truly were more 3rd order in nature than 2nd order (i.e. just as was obtained for the Mie case above). What is not clear is whether this spectral behavior can be truly ascribed to aerosol properties or, for example, to a systematic NIR channel artifact.

If we focus on the (AERONET standard) 2nd order polynomial results one sees a general trend of increasing errors when the wavelength sets are too clustered at the short or large wavelength ends of the "Ref." wavelength spectral region. Referring specifically to the 3 and 4-band, non-1020 nm channel results we can state that in order to avoid the excessively large $\Delta\tau_f$ cases of "e", "k", "p", and "q" ($\Delta\tau_f > 0.03$), it must stipulated that,

[8] the so called "rogue" filter set of {440, 532, 675, 870} nm, for example, represents a configuration which is close to a simple elimination of the 380 nm channel

for the chosen band set, one band must be 870 nm and one band must be less than or equal to 500 nm[9].

		5 wavlengths				4 wavlengths						3 wavlengths						
	Ref.	Stan.																
	380	**380**	**380**	**380**	380	**380**	**380**	**380**	**380**	380	380	380	380	**380**	380	380	380	**380**
	440	**440**	**440**	440	**440**	**440**	440	**440**	**440**	**440**	440	440	440	440	**440**	**440**	**440**	**440**
	500	**500**	500	**500**	**500**	**500**	**500**	500	**500**	**500**	**500**	500	**500**	500	500	**500**	**500**	**500**
	675	**675**	**675**	**675**	**675**	**675**	**675**	**675**	675	**675**	**675**	**675**	**675**	**675**	**675**	675	**675**	675
	870	**870**	**870**	**870**	**870**	870	**870**	**870**	**870**	**870**	**870**	**870**	**870**	**870**	**870**	**870**	870	870
	1020	1020	**1020**	**1020**	**1020**	1020	1020	1020	1020	1020	**1020**	**1020**	1020	1020	1020	1020	1020	1020
		a	b	c	d	e	f	g	h	i	j	k	l	m	n	o	p	q
$\Delta\tau_f$	2nd order	0.016	0.004	0.002	0.002	0.044	0.014	0.011	0.026	0.008	0.006	0.05	0.008	0.005	0.005	0.017	0.032	0.073
$\Delta\tau_f$	3rd order	0.005	0.004	0.004	0.012	0.006	0.004	0.009	0.016	0.011	0.018	N/A	N/A	N/A	N/A	N/A	N/A	N/A

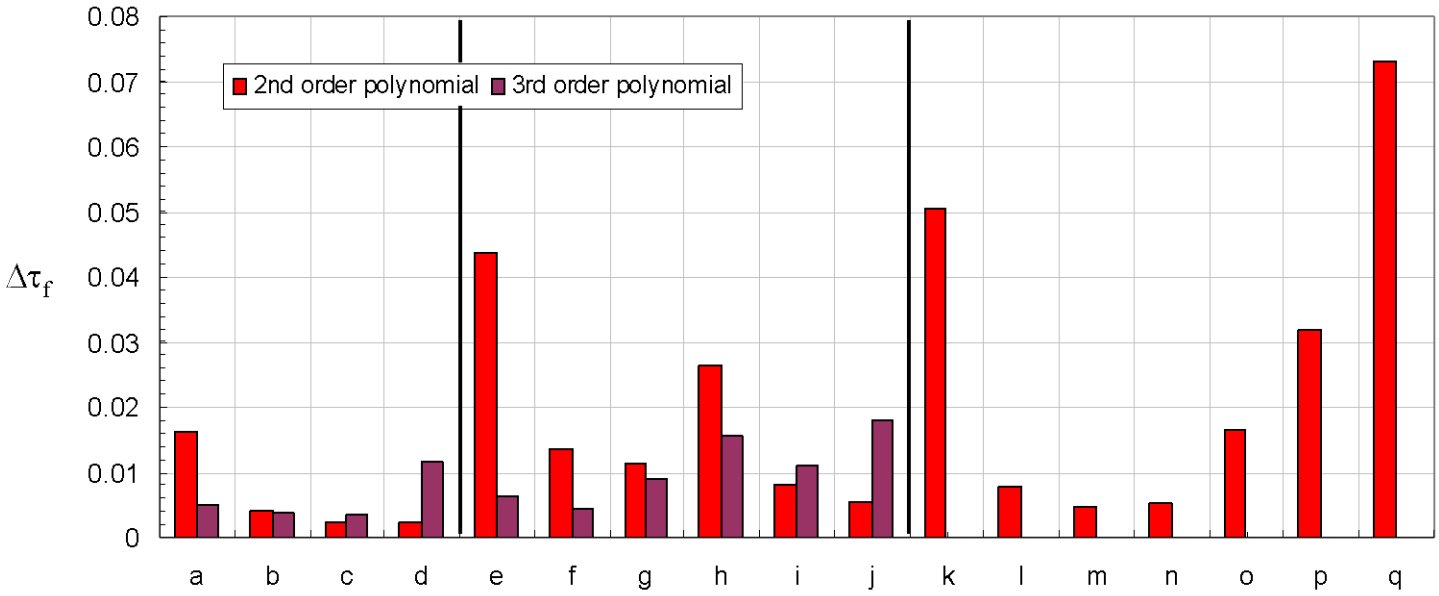

Fig. 5 - RMS differences in retrieved τ_f for different band sets (shown as bold type face in the table) relative to the 6 wavelength "Ref." band set. The labels "2nd order" and "3rd order" refer to the spectral polynomial which is regressed through the AODs as part of the SDA retrieval process (2nd order being the standard for AERONET). Filter sets with only 3 bands ("3 wavelengths") show no results for a 3rd order polynomial because the polynomial regression, in that case, is indeterminate for 3 wavelengths. These statistics were derived for Hornsund level 1.0 data acquired in March, 2008 (N = 313 AOD spectra). Level 1.5 (cloud filtered, N = 151) results were quite similar.

[9] The relatively large error for case "h" (2nd order polynomial) is clearly somewhat anomalous within this broad strategic context. Observations of sample spectra indicated that this was due to small but significant changes in curvature (α') as a function of the different filter sets (in other words it was not due to some anomaly induced by retrieval assumptions).

Channels employed in AERONET SDA processing

After an internal AERONET exchange followed by further tests on a variety of data sets, the following filter sets and processing conditions were defined for SDA AERONET processing. Some of the conditions were inspired by the Eureka work as well as the reduced-filter analysis of the previous section. The conditions inspired by tests carried out after the internal AERONET exchange are underlined.

Level 1.0

Standard: 380, 440, 500, 675, 870
SeaPRISM: 412, 443, 500, 555, 678, 870
Extended: 380, 440, 500, 675, 870
Rogue: 440, 532, 675, 870
- if any AOD is < 0.01 then eliminate that channel.
- if less than 3 channels remain then eliminate the whole AOD spectrum at that particular time[10]. One channel must be 870 nm and one channel must be 500 nm or less.
- polarization instruments (440, 675, 870) are excluded[11]

Level 1.5 and 2.0

Standard: 380, 440, 500, 675, 870
SeaPRISM: 412, 443, 500, 555, 678, 870
Extended: 380, 440, 500, 675, 870
Rogue: 440, 532, 675, 870
- if any AOD is < 0.02 then eliminate that channel (airmass <= 2) . If any AOD is < 0.02/(m*0.5) then eliminate that channel (airmass > 2).[12]
- if less than 3 channels remain then eliminate the whole AOD spectrum at that particular time. One channel must be 870 nm and one channel must be 500 nm or less.

Resolution of MOE problems in Version 4.0

MOE problems

[10] this is actually a processing chain requirement and not an option; for the standard 2nd order polynomial fit applied in the AERONET processing chain the regression procedure is indeterminate for less than 3 channels

[11] Extract of an Email dated April 24, 2007 from Ilya Slutsker; "The bug is fixed now. It was associated with Polarized device using those extra 870 polarized channels, that were not good in this example. From now we only use non-polarized channels for SDA retrievals."

[12] The figure originally proposed here was 0.03 rather than 0.02. A test performed for (very small AOD) data from PEARL (2007) indicated that a small but significant proportion of this data would be filtered out using the 0.03 value (at 500 nm) and none would be filtered out using the 0.02 value. The latter value corresponds to a reasonable "signal to noise" requirement of;

$AOD / (0.01/m) > 4$ (an alternative means of expressing the requirement that $AOD > 0.02/(0.5*m)$)

A problem with the Version 3.0 MOE (Mean of Extrema) algorithm was an over sensitivity to the estimated error bars in α_f (and in consequence η, τ_f and τ_c). It will be recalled that, in the MOE algorithm, the estimated error bars in α_f were employed to achieve a smooth transition in the forcing condition ($\eta \leq 1$). However it became apparent when processing large AOD smoke data over the Mongu site (Tom Eck) that this (a) created a situation where η values rarely got close to unity because the stochastic error estimates are typically quite large and (b) induced a ceiling effect in η and consequently a strong correlation was created between τ_f and τ_c (which wasn't a problem before the MOE type of error bar forcing). Figure 6 shows a particularly illustrative example of this effect in the Mongu data of 2004.

A second more minor problem was that the empirically developed stochastic expression for the rms error in α' was found to be more complicated than was merited (a much simpler expression was found to reproduce, about equally well, the empirical results of the stochastic simulations of the processing of an ensemble of noisy AOD spectra). This new rms expression was;

$$\Delta\alpha' = 10\ \sigma(\tau_a)/\tau_a$$

where $\sigma(\tau_a)$ is the rms error in the polynomial-fitted AOD.

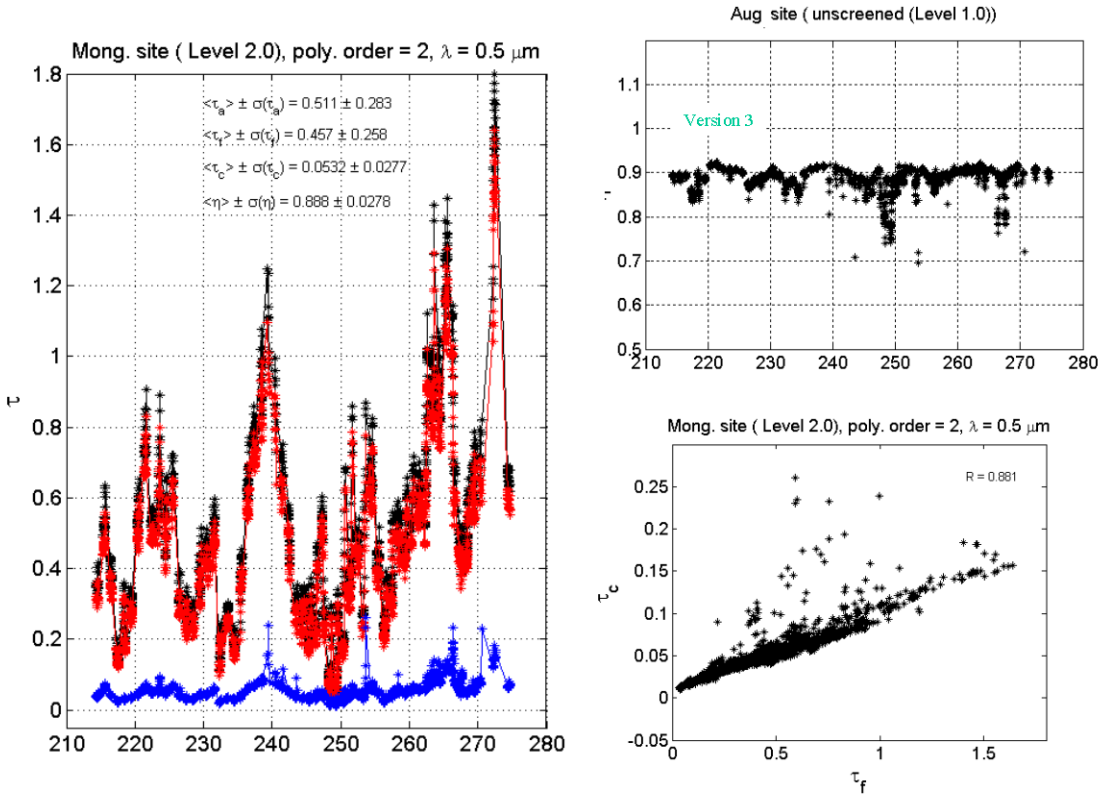

Figure 6 - Artificial correlation between τ_c and τ_f and ceiling effect in η induced by the Version 3.0 (MOE) physical forcing when η is near unity.

Resolution of MOE problems

A more general representation of the type of weighted averaging which occurs when $\eta \rightarrow 1$ (which includes the MOE) case is[13];

$$\alpha_f(\alpha_f^{(1)}) = \omega(\alpha_f^{(1)}) \alpha + [1 - \omega(\alpha_f^{(1)})] (\alpha_f^{(1)} + \Delta\alpha_f)$$

where $\alpha_f^{(1)}$ is the uncorrected estimate of α_f, $\alpha_f(\alpha_f^{(1)})$ is the corrected estimate, $\omega(\alpha_f^{(1)})$ is a weighting function and $\Delta\alpha_f$ is the estimated rms error in α_f. The pragmatic approach to eliminating the problem discussed above is to weight the recomputed αf mean more towards α (towards $\eta = 1$) than $\alpha f^{(1)} + \Delta\alpha_f$ rather than a straight unweighted mean between the same two quantities as was done for the MOE (Mean of Extrema approach) method of Versions 2 and 3 (and the same idea for the $\eta = 0$ forcing). This means $\omega(\alpha_f^{(1)}) > 0.5$ (where $\omega(\alpha_f^{(1)}) = 0.5$ for the MOE approach). The justification is that the part of the normal curve below $\alpha_f^{(1)} = \alpha$ should have some influence on the corrected α_f value (as opposed to none at all in the MOE). The details of this correction in terms of the analytical development of the quadratic expression for;

$$\omega(\alpha_f^{(1)}) = b_0 + b_1\alpha_f^{(1)} + b_2[\alpha_f^{(1)}]^2$$

and the 3rd order expression for $\alpha_f(\alpha_f^{(1)})$ are available from Norm O'Neill. Figure 7 shows how the effects of correlation between τ_c and τ_f and the ceiling effect in η is significantly reduced with the application of the Version 4.0 algorithm. This result is very similar to turning physical forcing off (without the infringements of the $\eta = [0, 1]$ limits which plague the case of no physical forcing); in other words, virtually no new correlation is induced by the algorithm. The residual correlation could well be real (coarse mode smoke being generated at the same time as fine mode smoke particles).

Figure 8 shows a schematic of the Version 3.0 and Version 4.0 averaging schemes.

[13] a similar approach was taken when $\eta \rightarrow 0$

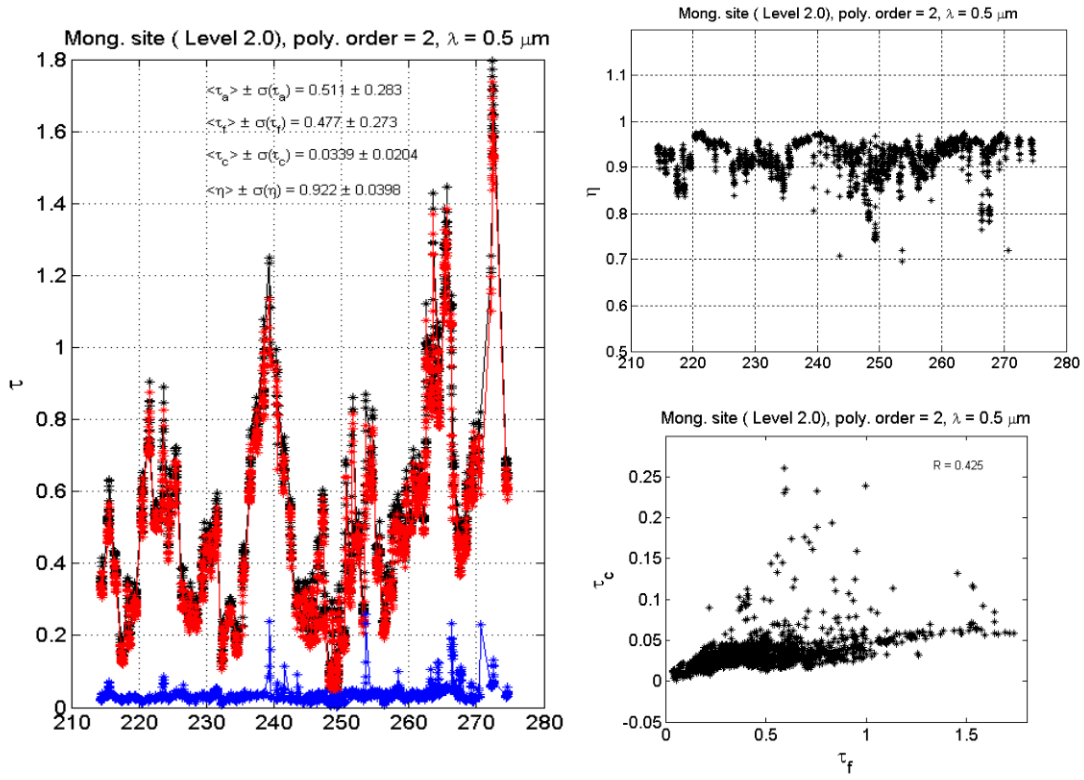

Figure 7 - Significantly reduced correlation between τ_c and τ_f using Version 4.0 algorithm.

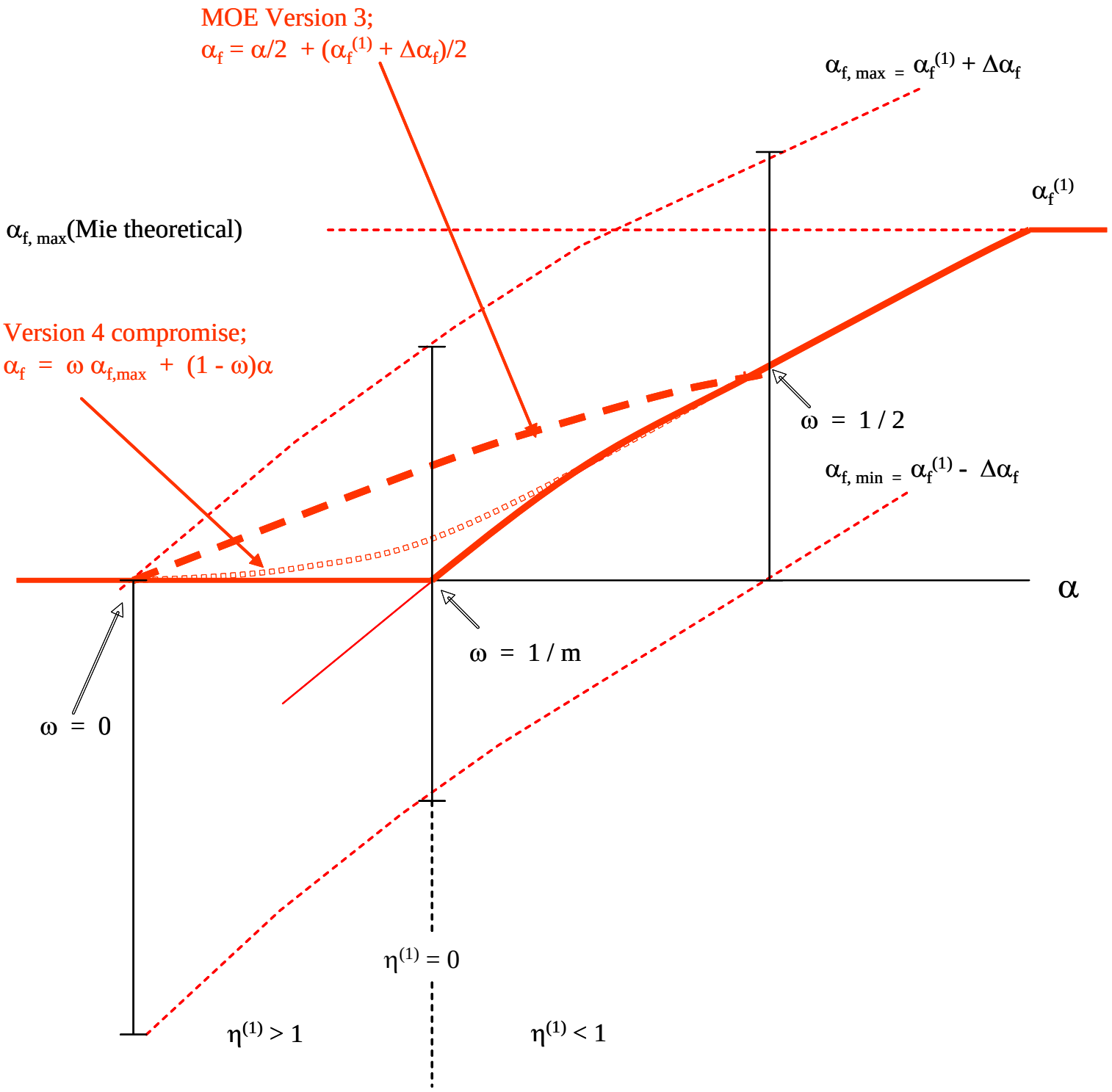

Figure 8 - Conceptual physical forcing illustration for the Version 3 and Version 4 algorithms. The solid vertical lines are the error bars in α_f. The dotted red line is the Version 3.0 (MOE) solution while the dashed bold red line is the Version 4.0 (quadratic weighting) solution. The superscript (1) refers to the uncorrected solution. The bold solid red line is the brute force correction without any error smoothing while the (non-bold) solid red line (mostly hidden by the bold solid red line) is the uncorrected solution. The parameter m = 8.

Retrieval Errors (stochastic error model)

A stochastic error model (which basically remained the same for all retrieval versions) yields an error estimate for all retrieved parameters (O'Neill et al., 2003). It is worth describing the qualitative features of the retrieval errors in terms of the SDA output parameters and the key intermediate parameter of α_f. With respect to pure Mie simulations, the stochastic error model results are illustrated in Figure 9[14] (in this simulation the fine mode optical depth increases geometrically with increasing value of the artificial time index). The (stochastic) error bars show several universal features; $\Delta\alpha_f$ increases with decreasing η since there is simply less significant fine mode "signal" available for its retrieval (between the extremes of $\alpha_f = \alpha$ for $\eta = 1$ and $\alpha_c = \alpha$ for $\eta = 0$). This trend is reversed in $\Delta\eta$ where the decreasing amplitude of η damps out the impact of the increase in $\Delta\alpha_f$ (to the point where $\Delta\eta$ actually decreases with decreasing η; it being recalled from ref. 2 that $\eta = [\alpha - \alpha_c] / [\alpha_f - \alpha_c]$). The moderately increasing value of $\Delta\eta$ with η combined with the increasing value of τ_a means that both $\Delta\tau_f \sim \Delta\eta\ \tau_a$ and $\Delta\tau_c \sim |\ \Delta\eta\ \tau_a\ |$ increase fairly rapidly with increasing η.

The stochastic error model does not and cannot account for irregularities in the measured AOD spectra which extend outside the limits of the nominal AERONET errors (rms errors < 0.01 to 0.02 for all channels) nor can it (or the retrieval algorithm) be expected to adequately deal with extremely non-Mie behavior such as a 1020 nm AOD which is significantly greater than lower-wavelength AODs (aerosol optical depths). Thus, for example, the small values of $\Delta\tau_f$ and $\Delta\tau_c$ seen in Fig. 9 for small τ_a (small η) can be artificial since this is precisely the region where fixed errors in τ_a play havoc with retrievals obtained from weak-valued τ_a spectra.

[14] This work was done before the error model changes discussed in the section entitle "Minor modificatioins to the code" above. Figure 9 changed very little after the code changes.

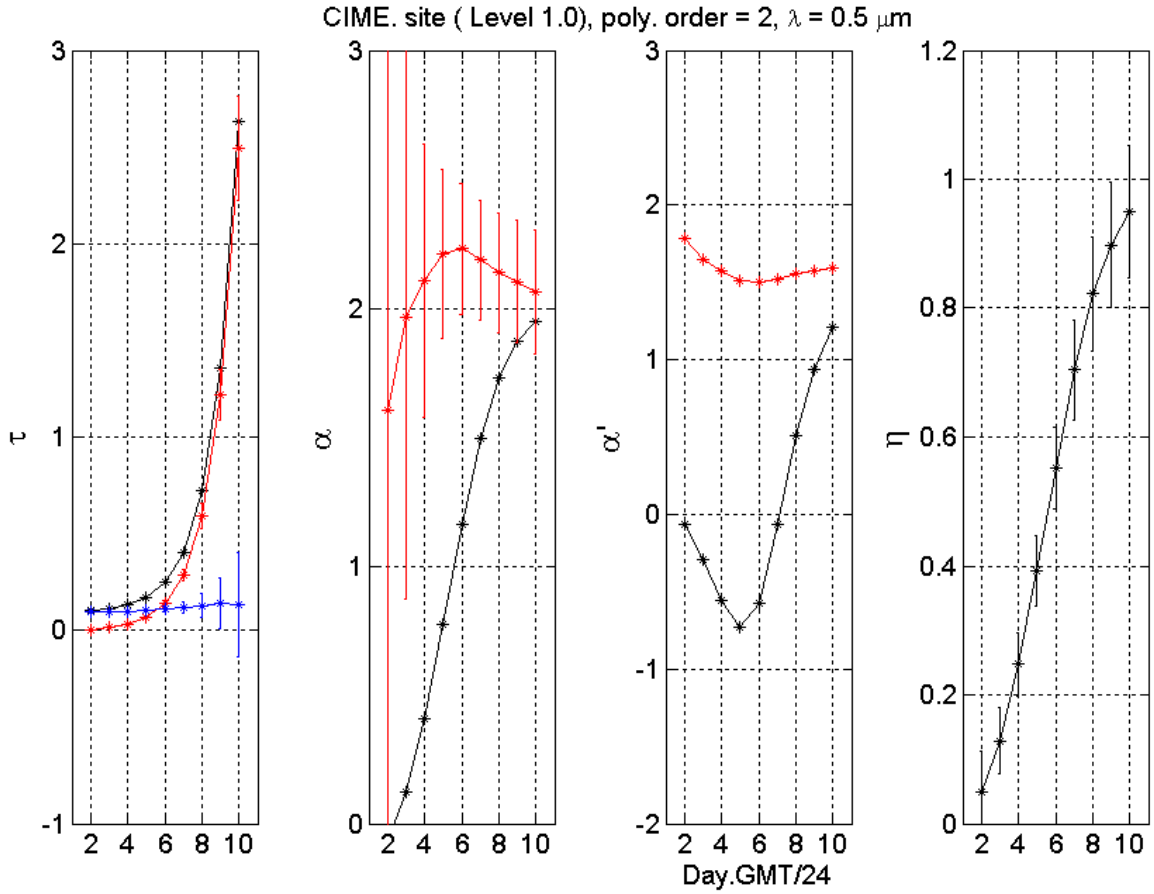

Figure 9 - Stochastic error results for simulated Mie retrievals (small fine-mode particle case; see first author for details)

Version 3.0

In March of 2005 Version 3.0 of tauf_tauc.m, to be implemented in the new AERONET processing system (called Version 2.0) was delivered. The problems which motivated a new version and the solutions effected are detailed below.

Version 2.0 problems to be resolved

(i) Version 2.0 still produced anomalous values for very large input AOD errors (discovered when the algorithm was applied to airborne AOD data which had nominal AOD errors >> nominal CIMEL AOD errors) : for very large AOD errors the "mean of extrema correction" was appropriately limited at the lower bound but there simply was no analogous upper bound when the uncertainty limits of α_f were up in the stratosphere (induced by overly large AOD errors) and thus the corrected value of α_f was excessively large (and in consequence the η values were too small).

(ii) The $\alpha_f' = f(\alpha_f)$ polynomial was moderately biased because it didn't include sufficiently small fine-mode PSD standard deviation cases in its envelope of uncertainty and because the original relationship (equation (7) of *O'Neill et al.* [2001b]) was not wavelength dependent when clearly it should be.

Resolution of Version 2.0 problems in Version 3.0

Version 3.0 of the spectral deconvolution algorithm was different from the Sept. 8 (Version 2.0) algorithm in the following ways ;

(i) physical forcing was rendered "symmetrical" in Version 3.0 by applying it to the upper as well as the lower physical bounds of α_f (the upper bounds, $\alpha_{f,max,\ theoretical}$ being spectrally dependent and ~ 3.5 as determined by Mie considerations).
(ii) New spectrally dependent coefficients of the parabola in equation (7) of O'Neill et al. [2001b] were employed. These are;

$a_{upper} = -.22, \quad b_{upper} = 10^{-0.2388}\,\lambda^{1.0275}, \quad c_{upper} = 10^{0.2633} * \lambda^{-0.4683}$
$a_{lower} = -.3, \quad b_{lower} = .8, \quad c_{lower} = .63$
$a = (a_{lower} + a_{upper})/2, \quad b = (b_{lower} + b_{upper})/2 \quad et \quad c = (c_{lower} + c_{upper})/2$

where the indices "upper" and "lower" refer to the uncertainties in the coefficients (due to uncertainty in the actual fine mode model). The new uncertainty in α_f (which propagates into the uncertainty in α_f, η, etc.) follows from these expressions, viz;

$$\Delta\alpha'_f = (a_{upper} - a_{lower})/2\ \alpha_f^2 + (b_{upper} - b_{lower})/2\ \alpha_f + (c_{upper} - c_{lower})/2.$$

Remaining problem in Version 3.0

The version 3.0 algorithm does not account for rare cases where $\alpha > \alpha_{f,max,\ theoretical}$ (usually associated with a serious artifact in one of the AOD channels). The solution

would mean forcing α to be = $\alpha_{f,max,\ theoretical}$. Rather than changing measurement values (up to this point only inverted values have been modified) it was decided to simply accept the infrequent occurence of this situation (for which $\eta > 1$).

Version 2.0 algorithm

Version 3.0 algorithm

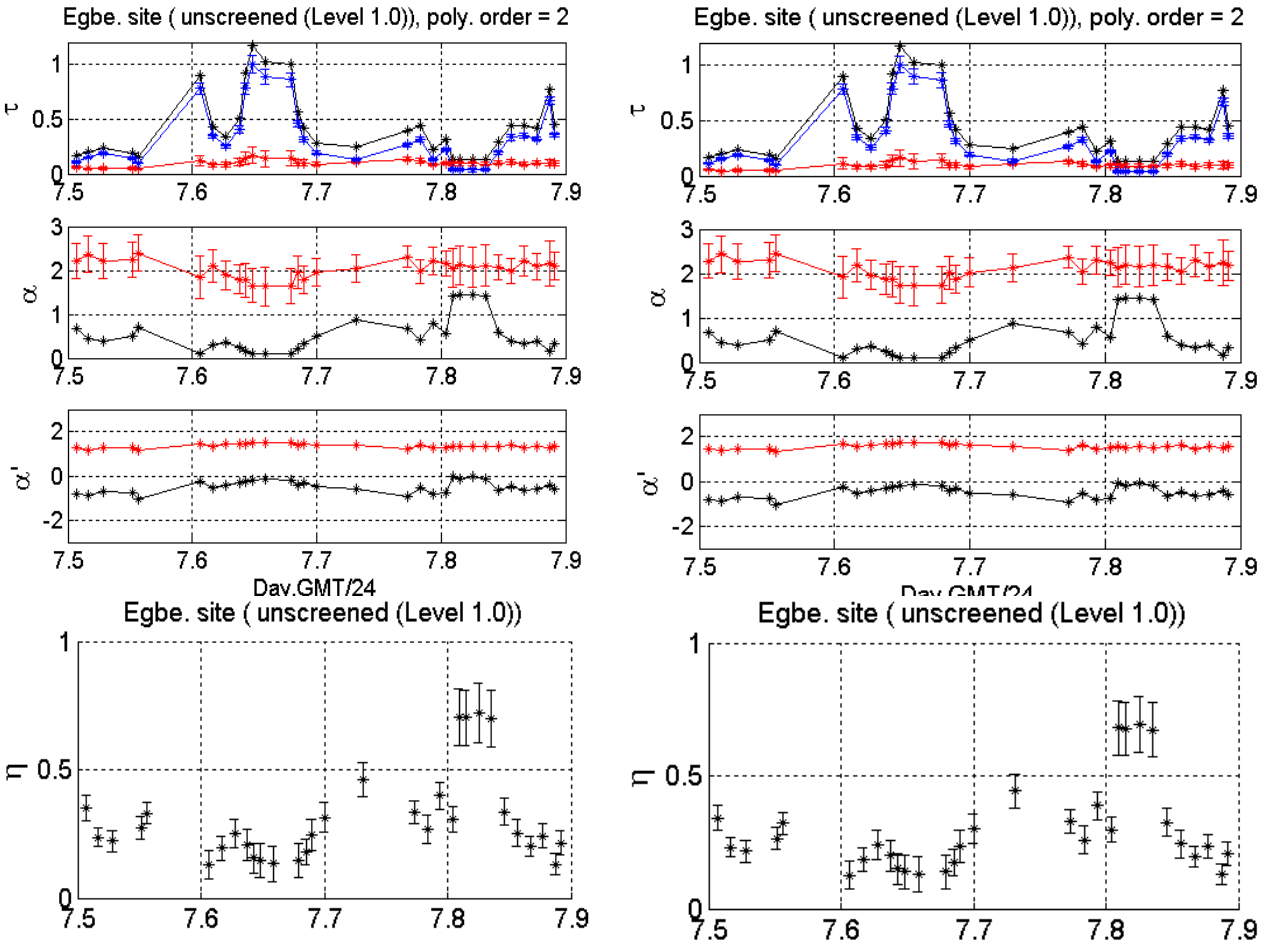

Figure 10 - Version 2.0 and version 3.0 spectral deconvolution results for Egbert, Ontario, Canada (λ = 500 nm). These results are for the same input data employed to produce Figure 4 of *O'Neill et al*. [2003].

Some comparative results

Figure 11 shows a comparison between Version 2.0 and Version 3.0 results. In this case the changes are very small (as they are also relative to Version 1.0 results shown in Figure 4 of *O'Neill et al*. [2003]).

Version 2.0 algorithm

Version 3.0 algorithm

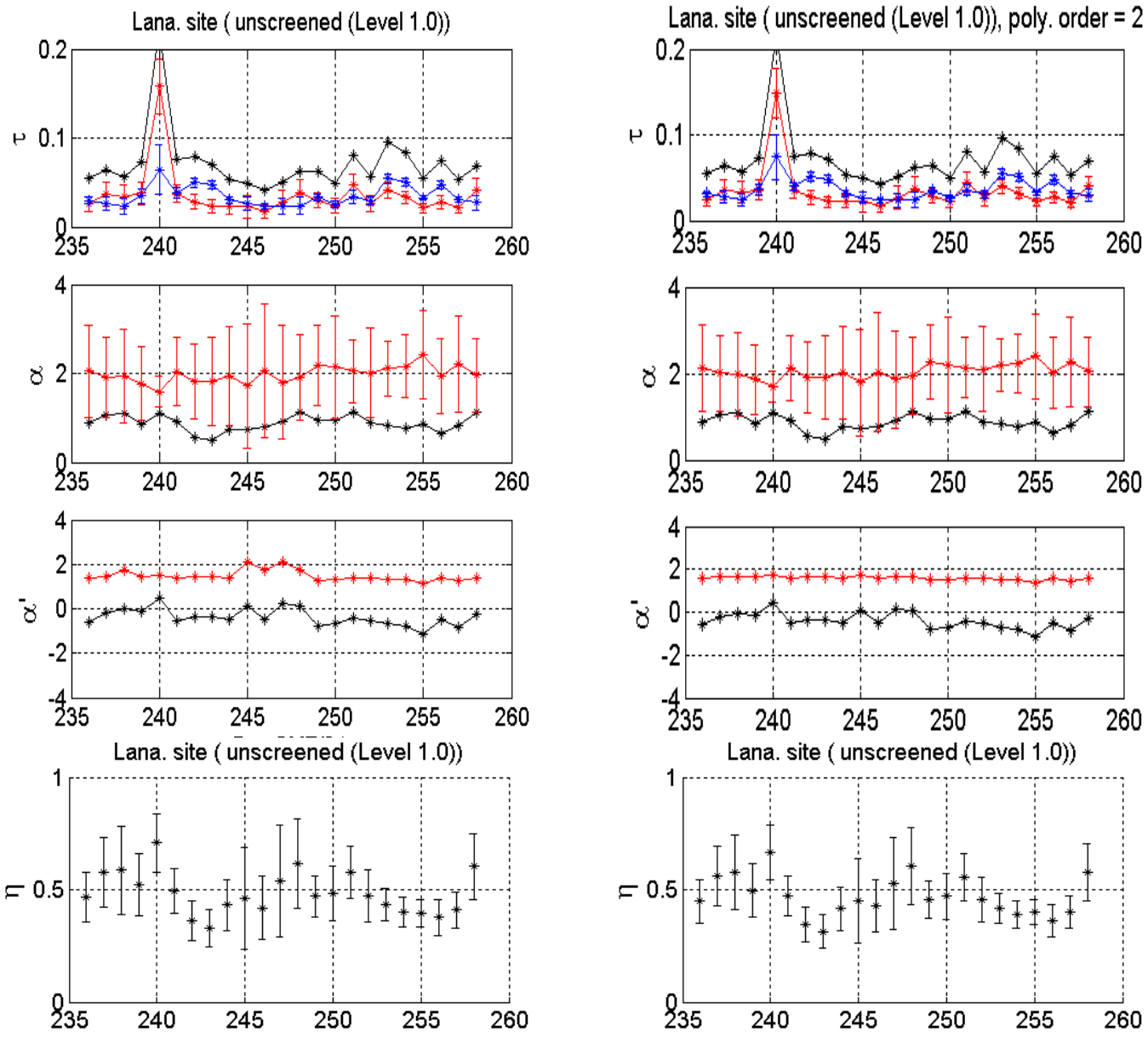

Figure 11 - Version 2.0 and version 3.0 spectral deconvolution results for the Lanai, Hawaii, site, Aug.-Sep 2001, λ = 550 nm (daily averages).

Figure 12 below shows a case where there are slightly more significant changes between the algorithms. Comparison with the Version 1.0 results of Figure 8 in *O'Neill et al.* [2003]) show that the anamolous AOD and Angstrom results of that figure (where $\tau_f > \tau_a$ and $\alpha_f < \alpha$) have appropriately disappeared. The modelled stochastic errors increase moderately from Version 2.0 to Version 3.0 while the nominal α_f and η values decrease and increase respectively by a small amount. Both versions demonstrate the progressively larger errors which one obtains as α_f decreases towards unity (as one approaches large fine mode particles).

Version 2.0 algorithm

Version 3.0 algorithm

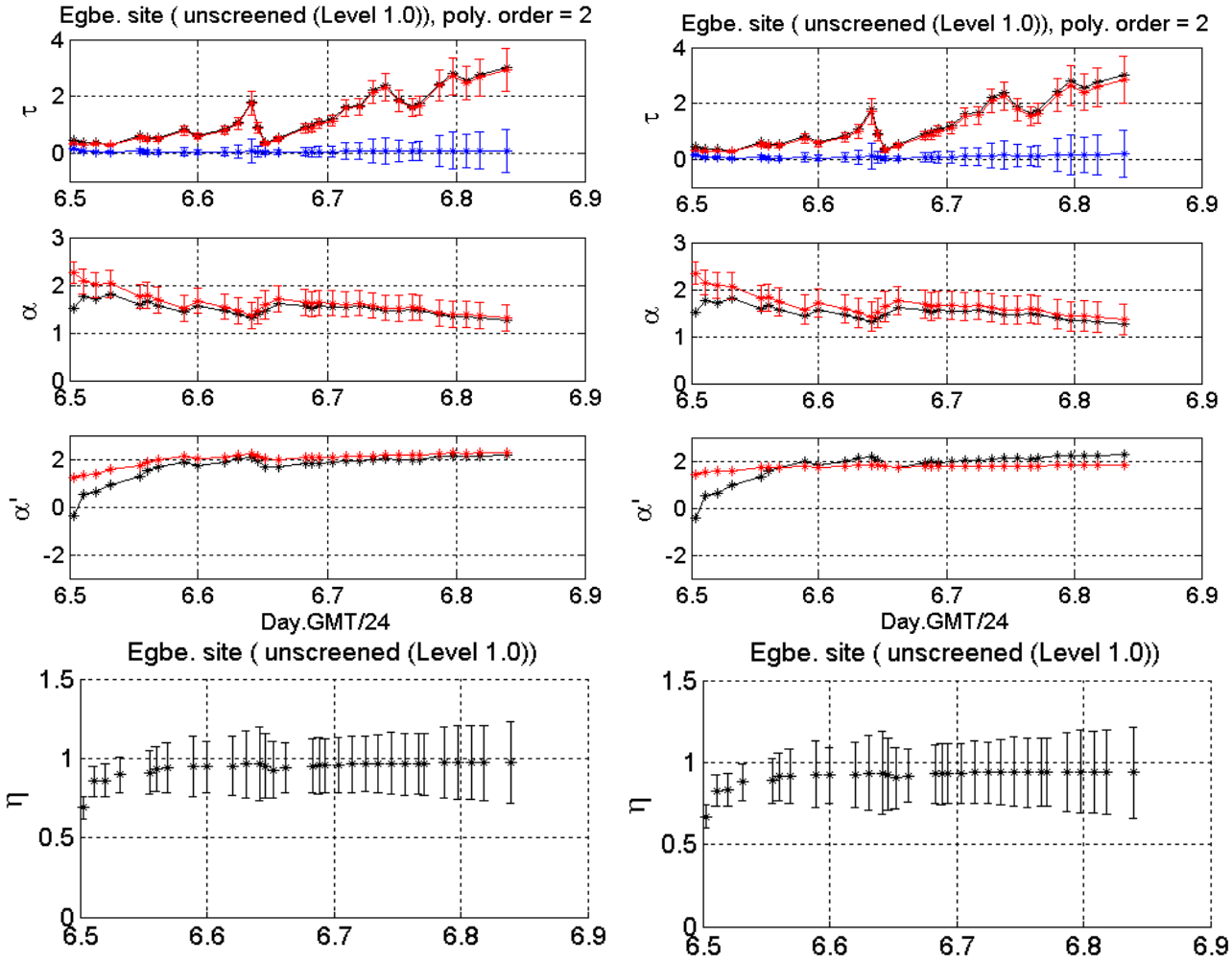

Figure 12 - Version 2.0 and version 3.0 spectral deconvolution results during the first day of the Québec smoke event of July 2002 at Egbert, Ontario, Canada (λ = 500 nm). These results are for the same input data employed to produce Figure 8 of *O'Neill et al.* [2003].

It was found that only extreme cases had any significant effect re the limit of $\alpha_{f,\ max,\ theoretical}$ on α_f. Figure 13 shows Version 2.0 versus 3.0 results for a case of very large AOD input error (precisely when one has problems with extremely large α_f values induced by very large uncertainty bars). It can be seen that the Version 3.0 α_f values are much more stable (which is in itself a positive thing) but that η values do not change by a lot except when the errors in α_f are quite exessive (measurements 1, 16, and 17 which are associated with anamolous artifacts in certain bands).

Version 2.0 algorithm

Version 3.0 algorithm

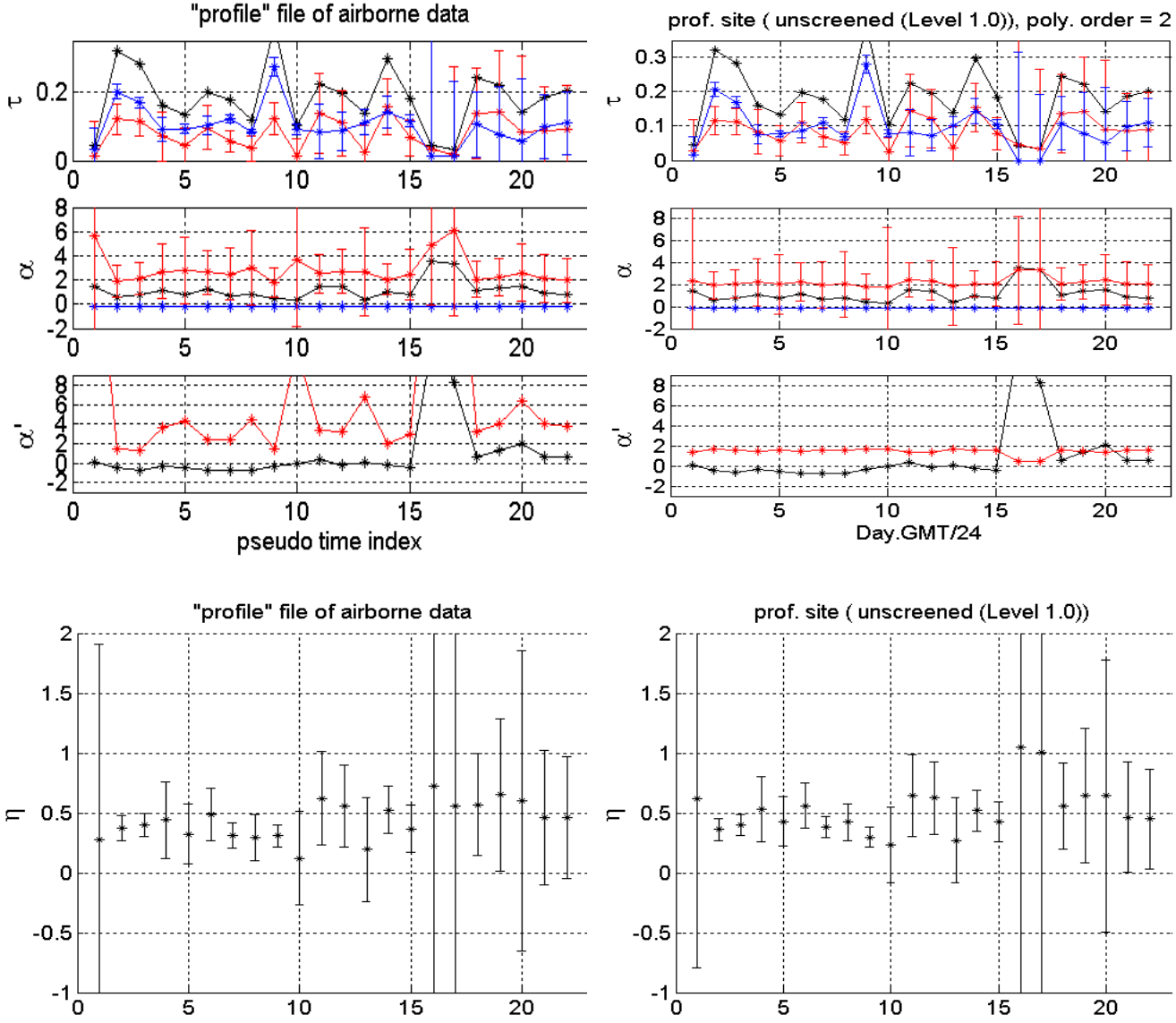

Figure 13 - Version 2.0 and version 3.0 spectral deconvolution results for some airborne data provided by Santiago Grasso. The nominal input AOD error is = 0.039 at a wavelength of λ = 0.55 μm. The x axis represents a measurement # index.

QA issues for Version 3.0

Data processing protocols typically include two or more levels which range from raw data to averaged value-added products. One could view the QA issue in the case of the spectral deconvolution algorithm as a choice between dynamic QA (where no points are eliminated but an error estimate is given for all points) and "pass / no-pass" type of filtering such as cloud screening. Below are some thoughts on each type.

Dynamic QA

The algorithm should be applied to level 1.0, 1.5 and 2.0 AOD since it is intended to discriminate coarse mode from fine mode AODs. In a very real sense it "rides" on the AERONET QA already in place; one could certainly speak of level 1.0, 1.5 and 2.0 values of τ_f, τ_c, and η.

Its not clear that a complementary QA process is necessary in the sense of pass/no-pass filter; the algorithm already provides a dynamic esimation of stochastic error ($\Delta\tau_f$, $\Delta\tau_c$, $\Delta\eta$) for every single AOD spectrum. There is not yet an analogue to this in Oleg's inversion processing because there is no provision for a dynamic error estimate of the derived products (and of course its much more complicated to do). As well, the physical forcing modifications of Version 3.0 have eliminated virtually all cases of non-physical values.

Pass / no-pass type of QA filter

If it is deemed essential to have pass / no-pass type of QA filter then possible candidates would be a combination of the two conditions below. The filter thresholds selected below represent a fairly liberal constraint while ensuring that extreme anomolies are eliminated.

- a threshold on the estimated stochastic error in $\Delta\tau_f$, $\Delta\tau_c$, $\Delta\eta$ ($\Delta\eta < 0.5$ would be a reasonable choice)
- some threshold on the AOD polynomial regression error $\Delta\tau_a / \tau_a$ (an indicator of how distorted the AOD spectrum is). $\Delta\tau_a / \tau_a < 0.3$ would be a liberal choice.

Relationship with Dubovic inversion outputs

The differences between the spectral deconvolution algorithm and the fine-mode / coarse-mode optical depths from the Dubovik inversion are, to a degree, expected since the current Dubovik output is the equivalent of what the community calls SMF (sub-micron fraction) as opposed to the spectral deconvolution algorithm output which is essentially an FMF (fine mode fraction) type of discrimination[15]. The former is a purely mechanical cutoff in radius (which is fundamentally how mechanical discriminators work) while the latter is a total mode discrimination (arguably more physically fundamental in that the different modes represent different physical origins). This means that $\tau_{c,\,SM} < \tau_{c,\,FM}$ so that $\tau_{f,\,SM} > \tau_{f,\,FM}$ and hence SMF > FMF ($\eta_{SM} > \eta_{FM}$). The new Dubovik inversion which will base the fine-mode / coarse-mode division on the

[15] the spectral deconvolution approach is really spectral in nature (one assumes apriori properties of the coarse mode spectrum). This spectral approach is much more closely tied with the FMF than the SMF. In terms of the notation in O'Neill et al. (2003), FMF = η.

minimum value of the (volume) particle size distribution value rather than the current 0.6 μm cutoff will be more analogous to a FMF type of division.

Version 2.0

On or about Sept. 8, 2004 a new tauf_tauc.m version with a "physical_forcing" option for eliminating $\eta > 1$ problems was delivered to AERONET. Details are given below.

Problems resolved with respect to the Version 1.0 algorithm

Under certain conditions the value of the ("monochromatic") Angstrom exponent (α) exceeded the maximum value of α_f permitted by equation (7) of O'Neill et al., (2001b). This automatically created a non-physical situation where the fine mode fraction (η) was greater than unity (and the spectral derivative α' was as a consequence greater than α_f'). These conditions usually corresponded to cases of thick, aged (large particle) smoke when α' was large and α was small. The problem was fixed in a smoothly varying fashion by implementing the "physical forcing" option described in the section immediately below.

Resolution of Version 1.0 problems in Version 2.0

If any portion of the uncertainty bar of α_f (computed from the stochastic error estimate described in O'Neill et al., 2001b) was lower than α then a new value of α_f was computed as the mean of the upper extrema of the estimated α_f uncertainty and α. This "mean of extrema" (MOE) modification is represented by the dotted line in Figure 8.

Version 1.0

This is basically the algorithm described in O'Neill et al., 2001b and O'Neill et al., 2003 and it was the first algorithm delivered to AERONET (to Ilya Slutsker).

Appendix A: differential and quadrature expressions employed in the stochastic error model

This Appendix replaces Appendix A of O'Neill et al. (2003) (although the expression for $\Delta\alpha'_{bias}$ given in Appendix A.1 is still applicable).

Differential expressions for α_f and η

We have from simulate_CIMEL_errors.ppt that $\Delta\alpha \approx -2.5\,\Delta\tau/\tau = k_2\,\Delta\tau_a/\tau_a$, $\Delta\alpha' \approx -4\,\Delta\alpha$ and by combination that $\Delta\alpha' \approx 10\,\Delta\tau_a/\tau_a = k_1\,\Delta\tau_a/\tau_a$. We have from O'Neill et al. (2001);

$$d\alpha_f = \frac{\partial\alpha_f}{\partial\alpha'}\Delta\alpha' + \frac{\partial\alpha_f}{\partial\alpha}\Delta\alpha + \frac{\partial\alpha_f}{\partial\alpha'_f}\Delta\alpha'_f + \frac{\partial\alpha_f}{\partial\alpha'_c}\Delta\alpha'_c + \frac{\partial\alpha_f}{\partial\alpha_c}\Delta\alpha_c$$

$$d\eta = \frac{\partial\eta}{\partial\alpha'}\Delta\alpha' + \frac{\partial\eta}{\partial\alpha}\Delta\alpha + \frac{\partial\eta}{\partial\alpha'_f}\Delta\alpha'_f + \frac{\partial\eta}{\partial\alpha'_c}\Delta\alpha'_c + \frac{\partial\eta}{\partial\alpha_c}\Delta\alpha_c$$

This really should have been in terms of explicit functionality of α_f (the α'_f error term represents an approximation). This explicit funtionality is given in O'Neill et al. (2001)[16];

$$\alpha_f - \alpha_c = \frac{1}{2(1-a)}\{t + b^* + D\} \quad \text{where}$$

$$D = \sqrt{(t + b^*)^2 + 4(1 - a)\,c^*}$$

$$b^* = b + 2\alpha_c\,a, \qquad c^* = c + (b + a\,\alpha_c)\alpha_c - \alpha_c'$$

$$t = \alpha - \alpha_c - \frac{\alpha' - \alpha_c'}{\alpha - \alpha_c}$$

and accordingly;

$$d\alpha_f = \frac{\partial\alpha_f}{\partial\alpha'}\Delta\alpha' + \frac{\partial\alpha_f}{\partial\alpha}\Delta\alpha + \frac{\partial\alpha_f}{\partial a}\Delta a + \frac{\partial\alpha_f}{\partial b}\Delta b + \frac{\partial\alpha_f}{\partial c}\Delta c + \frac{\partial\alpha_f}{\partial\alpha'_c}\Delta\alpha'_c + \frac{\partial\alpha_f}{\partial\alpha_c}\Delta\alpha_c$$

$$d\eta = \frac{\partial\eta}{\partial\alpha'}\Delta\alpha' + \frac{\partial\eta}{\partial\alpha}\Delta\alpha + \frac{\partial\eta}{\partial a}\Delta a + \frac{\partial\eta}{\partial b}\Delta b + \frac{\partial\eta}{\partial c}\Delta c + \frac{\partial\eta}{\partial\alpha'_c}\Delta\alpha'_c + \frac{\partial\eta}{\partial\alpha_c}\Delta\alpha_c$$

[16] except that the expression for b* in that paper is incorrect. The correct expression is given in this section.

The approach for computing the values of Δa, Δb, and Δc is given in visible.xls (sheet "AERONET"). At a wavelength of 0.5 μm the values are 0.04, -0.26 and 0.96 respectively. The rms values of $\Delta\alpha_c$ and $\Delta\alpha'_c$ were taken as 0.15 and 0.15 respectively.

Partial derivatives of α_f

From the above expressions;

$$\frac{\partial t}{\partial \alpha} = 1 + \frac{\alpha' - \alpha_c'}{(\alpha - \alpha_c)^2} = \frac{t_+}{\alpha - \alpha_c} \qquad \text{where } t_+ = \alpha - \alpha_c + \frac{\alpha' - \alpha_c'}{\alpha - \alpha_c}$$

$$\frac{\partial D}{\partial \alpha} = \frac{1}{2}\frac{1}{D}2(t + b^*)\frac{\partial t}{\partial \alpha} = \frac{(t + b^*)}{D}\frac{t_+}{\alpha - \alpha_c}$$

so that

$$\frac{\partial \alpha_f}{\partial \alpha} = \frac{1}{2(1 - a)}\left(\frac{\partial t}{\partial \alpha} + \frac{\partial D}{\partial \alpha}\right) = \frac{1}{2(1 - a)}\frac{t_+}{\alpha - \alpha_c}\left(1 + \frac{(t + b^*)}{D}\right)$$

$$= \frac{\alpha_f - \alpha_c}{\alpha - \alpha_c}\frac{t_+}{D} = \frac{t_+}{\eta D}$$

Does this make sense? The last equation can be alternatively expressed as;

$$\frac{\partial \alpha_f}{\partial \alpha} = \frac{t_+}{\eta((\alpha_f - \alpha_c)2(1 - a) - t - b^*)} = \frac{2(\alpha_f - \alpha) - t}{\eta(2(\alpha_f - \alpha_c) - t - 2a\alpha_f + 2a\alpha_c - b - 2a\alpha_c)}$$

$$= \frac{1}{\eta}\frac{2(\alpha_f - \alpha) - t}{(2(\alpha_f - \alpha_c) - t - (2a\alpha_f + b))}$$

To check this derivation we can derive it a slightly different fashion. From the "conservation of t" relation defined in O'Neill et al. (2001);

$$t = \alpha - \alpha_c - \frac{\alpha' - \alpha_c'}{\alpha - \alpha_c} = \alpha_f - \alpha_c - \frac{\alpha'_f - \alpha_c'}{\alpha_f - \alpha_c}$$

$$1 - (\alpha' - \alpha_c')\frac{(-1)}{(\alpha - \alpha_c)^2} = \frac{\partial \alpha_f}{\partial \alpha} - \frac{\frac{\partial \alpha'_f}{\partial \alpha_f}\frac{\partial \alpha_f}{\partial \alpha}}{\alpha_f - \alpha_c} - (\alpha'_f - \alpha_c')\frac{(-1)\frac{\partial \alpha_f}{\partial \alpha}}{(\alpha_f - \alpha_c)^2}$$

$$\frac{2(\alpha - \alpha_c) - t}{(\alpha - \alpha_c)} = \frac{\partial \alpha_f}{\partial \alpha}\left\{1 - \frac{1}{\alpha_f - \alpha_c}\left[\frac{\partial \alpha'_f}{\partial \alpha_f} - \frac{(\alpha'_f - \alpha_c')}{(\alpha_f - \alpha_c)}\right]\right\}$$

$$= \frac{\partial \alpha_f}{\partial \alpha}\frac{1}{\alpha_f - \alpha_c}\left\{2(\alpha_f - \alpha_c) - t - \frac{\partial \alpha'_f}{\partial \alpha_f}\right\}$$

$$\frac{\partial \alpha_f}{\partial \alpha} = \frac{1}{\eta}\frac{2(\alpha - \alpha_c) - t}{\left(2(\alpha_f - \alpha_c) - t - \frac{\partial \alpha'_f}{\partial \alpha_f}\right)}$$

which is the same as the result above given that the derivative of the expression for α'_f in terms of α_f (O'Neill et al., 2001) is;

$$\frac{\partial \alpha'_f}{\partial \alpha_f} = \frac{\partial\left(a\alpha_f^2 + b\alpha_f + c\right)}{\partial \alpha_f} = 2a\alpha_f + b$$

One would think that as $\eta \to 1$, $\alpha \to \alpha_f$ that $\partial\alpha_f / \partial\alpha \to 1$[17]. However this clearly is not the case; $\alpha \cong \alpha_f$ is too simplistic (one cannot ignore the 2nd derivative constraining equations[18]) in terms of predicting $\partial\alpha_f / \partial\alpha$.

[17] This would clearly be the case if α'_f was independent of α_f (or hence independent of α since $\alpha_f = f(\alpha)$).
[18] equation (3) in O'Neill et al. (2001)

Similarily;

$$\frac{\partial t}{\partial \alpha'} = \frac{-1}{\alpha - \alpha_c}$$

$$\frac{\partial D}{\partial \alpha'} = \frac{1}{2}\frac{1}{D}2(t + b^*)\frac{\partial t}{\partial \alpha'} = -\frac{(t + b^*)}{D}\frac{1}{\alpha - \alpha_c}$$

so that

$$\frac{\partial \alpha_f}{\partial \alpha'} = \frac{1}{2(1 - a)}\left(\frac{\partial t}{\partial \alpha'} + \frac{\partial D}{\partial \alpha'}\right) = \frac{1}{2(1 - a)}\frac{-1}{\alpha - \alpha_c}\left(1 + \frac{(t + b^*)}{D}\right)$$

$$= \frac{\alpha_f - \alpha_c}{\alpha - \alpha_c}\left(\frac{-1}{D}\right) = \frac{-1}{\eta D}$$

The partial derivative relative to α_c is[19];

$$\frac{\partial \alpha_f}{\partial \alpha_c} = 1 + \frac{1}{2(1-a)}\left\{\frac{\partial t}{\partial \alpha_c} + \frac{\partial b^*}{\partial \alpha_c} + \frac{\partial D}{\partial \alpha_c}\right\}$$

where $\frac{\partial t}{\partial \alpha_c} = \frac{-t_+}{\alpha - \alpha_c}$, $\frac{\partial b^*}{\partial \alpha_c} = 2a$, $\frac{\partial c^*}{\partial \alpha_c} = b + 2a\alpha_c = b^*$ and

$$\frac{\partial D}{\partial \alpha_c} = \frac{1}{D}\left[(t + b^*)\left(\frac{\partial t}{\partial \alpha_c} + 2a\right) + 2(1-a)b^*\right], \text{ so that}$$

$$\frac{\partial \alpha_f}{\partial \alpha_c} = 1 + \frac{1}{2(1-a)}\left\{\frac{\partial t}{\partial \alpha_c} + 2a + \frac{1}{D}\left[(t + b^*)\left(\frac{\partial t}{\partial \alpha_c} + 2a\right) + 2(1-a)b^*\right]\right\}$$

[19] corrected on on Mar. 27, 2008 (relative to O'Neill et al., (2003)) for a missing $\partial D / \partial \alpha_c$ term of $2(1-a)b/D$ and for an error in $\partial t / \partial \alpha_c$. In the latter case it is clear that $t(\alpha - \alpha_c) = -t(\alpha_c - \alpha)$ so that $\partial t(\alpha - \alpha_c) / \partial \alpha_c = -\partial t(\alpha_c - \alpha) / \partial \alpha_c$. But it is easy to see that the right hand expression is $= -\partial t(\alpha - \alpha_c) / \partial \alpha$ or more simply put $-\partial t / \partial \alpha$.

$$= 1 + \frac{1}{2(1-a)}\frac{1}{D}\left\{D\left(\frac{\partial t}{\partial \alpha_c} + 2a\right) + (t + b^*)\left(\frac{\partial t}{\partial \alpha_c} + 2a\right) + 2(1-a)(b + 2a\,\alpha_c)\right\}$$

$$= 1 + \frac{1}{2(1-a)}\frac{1}{D}\left\{(D + t + b^*)\left(\frac{\partial t}{\partial \alpha_c} + 2a\right) + 2(1-a)\,b^*\right\}$$

Now; $\frac{\partial t}{\partial \alpha_c} + 2a = \frac{-t_+}{\alpha - \alpha_c} + 2a = \frac{-(2(\alpha - \alpha_c) - t)}{\alpha - \alpha_c} + 2a = \frac{t}{\alpha - \alpha_c} - 2(1 - a)$, so that

$$\frac{\partial \alpha_f}{\partial \alpha_c} = \frac{1}{2(1-a)}\frac{1}{D}\left\{2(1-a)D + (D + t + b^*)\left(\frac{t}{\alpha - \alpha_c} - 2(1 - a)\right) + 2(1-a)\,b^*\right\}$$

$$= \frac{1}{2(1-a)}\frac{1}{D}\left\{(D + t + b^*)\left(\frac{t}{\alpha - \alpha_c}\right) - 2t(1 - a)\right\}$$

$$= \frac{1}{2(1-a)}\frac{1}{D}\left\{(\alpha_f - \alpha_c)2(1 - a)\left(\frac{t}{\alpha - \alpha_c}\right) - 2t(1 - a)\right\}$$

$$= \frac{t}{D}\left\{\frac{1}{\eta} - 1\right\}$$

$$\frac{\partial \alpha_f}{\partial \alpha_c'} = \frac{1}{2(1-a)}\left\{\frac{\partial t}{\partial \alpha_c'} + \frac{\partial D}{\partial \alpha_c'}\right\}$$

where $\frac{\partial t}{\partial \alpha_c'} = \frac{1}{\alpha - \alpha_c}$, and

$$\frac{\partial D}{\partial \alpha_c'} = \frac{1}{2}\frac{1}{D}\left[2(t + b^*)\frac{\partial t}{\partial \alpha_c'} + 4(1-a)\frac{\partial c^*}{\partial \alpha_c'}\right], \quad \frac{\partial c^*}{\partial \alpha_c'} = -1, \text{ so that}$$

$$\frac{\partial \alpha_f}{\partial \alpha_c'} = \frac{1}{2(1-a)}\left\{\frac{\partial t}{\partial \alpha_c'} + \frac{1}{D}\left[(t + b^*)\frac{\partial t}{\partial \alpha_c'} - 2(1-a)\right]\right\}$$

$$= \frac{1}{2(1-a)}\frac{1}{D}\left\{(D + t + b^*)\frac{\partial t}{\partial \alpha_c'} - 2(1-a)\right\}$$

$$= \frac{1}{2(1-a)}\frac{1}{D}\left\{2(1-a)(\alpha_f - \alpha_c)\frac{1}{\alpha - \alpha_c} - 2(1-a)\right\}$$

$$= \frac{1}{D}\left(\frac{1}{\eta} - 1\right)$$

Partial derivatives of a, b, c

We can express the general α_f solution as;

$$\alpha_f - \alpha_c = \frac{1}{2(1-a)}\{t + b^* + D\} = \frac{G}{2(1-a)}$$

where $G = y + D = y + \sqrt{y^2 + z}$ with $y = t + b^*$, $z = 4(1-a)c^*$

The derivatives of the component variables are;

(recalling that $b^* = b + 2\alpha_c a, c^* = c + (b + a\alpha_c)\alpha_c - \alpha_c'$)

$$\frac{\partial t}{\partial a} = 0 \quad \frac{\partial t}{\partial b} = 0 \quad \frac{\partial t}{\partial c} = 0$$
$$\frac{\partial b^*}{\partial a} = 2\alpha_c \quad \frac{\partial b^*}{\partial b} = 1 \quad \frac{\partial b^*}{\partial c} = 0$$
$$\frac{\partial c^*}{\partial a} = \alpha_c^{\,2} \quad \frac{\partial c^*}{\partial b} = \alpha_c \quad \frac{\partial c^*}{\partial c} = 1$$

So that;

$$\frac{\partial G}{\partial x} = \frac{\partial y}{\partial x} + \frac{1}{2D}\left(2y\frac{\partial y}{\partial x} + \frac{\partial z}{\partial x}\right)$$

$$= \frac{1}{D}\left(D\frac{\partial y}{\partial x} + y\frac{\partial y}{\partial x} + \frac{1}{2}\frac{\partial z}{\partial x}\right)$$

$$= \frac{1}{D}\left((\alpha_f - \alpha_c)\,2(1 - a)\frac{\partial y}{\partial x} + \frac{1}{2}\frac{\partial z}{\partial x}\right)$$

Applying this relationship to each separate constant;

$$\frac{\partial \alpha_f}{\partial b} = \frac{1}{2(1 - a)}\frac{\partial G}{\partial b} = \frac{1}{2(1 - a)}\frac{1}{D}\left((\alpha_f - \alpha_c)\,2(1 - a)\frac{\partial b^*}{\partial b} + \frac{1}{2}4(1 - a)\frac{\partial c^*}{\partial b}\right)$$

$$= \frac{1}{D}\left((\alpha_f - \alpha_c) + \alpha_c\right) = \frac{\alpha_f}{D}$$

$$\frac{\partial \alpha_f}{\partial c} = \frac{1}{2(1 - a)}\frac{\partial G}{\partial c} = \frac{1}{2(1 - a)}\frac{1}{D}\left((\alpha_f - \alpha_c)\,2(1 - a)\frac{\partial b^*}{\partial c} + \frac{1}{2}4(1 - a)\frac{\partial c^*}{\partial c}\right)$$

$$= \frac{1}{D}$$

$$\frac{\partial \alpha_f}{\partial a} = -\frac{G}{2}\frac{(-1)}{(1-a)^2} + \frac{1}{2(1-a)}\frac{\partial G}{\partial c}$$

$$= \frac{(\alpha_f - \alpha_c)}{(1-a)} + \frac{1}{2(1-a)}\frac{1}{D}\left((\alpha_f - \alpha_c)2(1-a)\frac{\partial b^*}{\partial a} + \frac{1}{2}4(1-a)\frac{\partial c^*}{\partial a} + \frac{1}{2}4c^*(-1)\right)$$

$$= \frac{(\alpha_f - \alpha_c)}{(1-a)} + \frac{1}{2(1-a)}\frac{1}{D}\left((\alpha_f - \alpha_c)2(1-a)2\alpha_c + 2(1-a)\alpha_c^2 - 2c^*\right)$$

$$= \frac{(\alpha_f - \alpha_c)}{(1-a)} + \frac{(\alpha_f - \alpha_c)}{D}2\alpha_c + \frac{\alpha_c^2}{D} - \frac{c^*}{(1-a)D}$$

$$= \frac{(\alpha_f - \alpha_c)}{(1-a)} + \frac{1}{D}\left(\alpha_c(2\alpha_f - \alpha_c) - \frac{c^*}{(1-a)}\right)$$

Partial derivatives of η

The differential in η is derived from the computational expression used to derive it;

$$\eta = \frac{\alpha - \alpha_c}{\alpha_f - \alpha_c}$$

$$d\eta = \frac{1}{\alpha_f - \alpha_c}\left(\Delta\alpha - \eta\Delta\alpha_f - (1-\eta)\Delta\alpha_c\right)$$

$$d\eta = \frac{1}{\alpha_f - \alpha_c}\left(\Delta\alpha - \eta\left\{\frac{\partial\alpha_f}{\partial\alpha'}\Delta\alpha' + \frac{\partial\alpha_f}{\partial\alpha}\Delta\alpha + \delta_{a,b,c} + \frac{\partial\alpha_f}{\partial\alpha'_c}\Delta\alpha'_c + \frac{\partial\alpha_f}{\partial\alpha_c}\Delta\alpha_c\right\} - (1-\eta)\Delta\alpha_c\right)$$

$$= \frac{1}{\alpha_f - \alpha_c}\left((1 - \eta\frac{\partial\alpha_f}{\partial\alpha})\Delta\alpha - \eta\frac{\partial\alpha_f}{\partial\alpha'}\Delta\alpha' - \eta\delta_{a,b,c} - \eta\frac{\partial\alpha_f}{\partial\alpha'_c}\Delta\alpha'_c - (1 - \eta + \eta\frac{\partial\alpha_f}{\partial\alpha_c})\Delta\alpha_c\right)$$

$$\text{where } \delta_{a,b,c} = \frac{\partial\alpha_f}{\partial a}\Delta a + \frac{\partial\alpha_f}{\partial b}\Delta b + \frac{\partial\alpha_f}{\partial c}\Delta c$$

From the above expression, the partial derivatives of η are given by;

$$\frac{\partial \eta}{\partial \alpha} = \frac{1 - \eta \frac{\partial \alpha_f}{\partial \alpha}}{\alpha_f - \alpha_c}$$

$$\frac{\partial \eta}{\partial \alpha'} = \frac{-\eta \frac{\partial \alpha_f}{\partial \alpha'}}{\alpha_f - \alpha_c},$$

$$\frac{\partial \eta}{\partial a} = \frac{-\eta \frac{\partial \alpha_f}{\partial a}}{\alpha_f - \alpha_c}, \frac{\partial \eta}{\partial b} = \frac{-\eta \frac{\partial \alpha_f}{\partial b}}{\alpha_f - \alpha_c}, \frac{\partial \eta}{\partial c} = \frac{-\eta \frac{\partial \alpha_f}{\partial c}}{\alpha_f - \alpha_c},$$

$$\frac{\partial \eta}{\partial \alpha'_c} = \frac{-\eta \frac{\partial \alpha_f}{\partial \alpha'_c}}{\alpha_f - \alpha_c}, \qquad \frac{\partial \eta}{\partial \alpha_c} = \frac{-\left(1 - \eta + \eta \frac{\partial \alpha_f}{\partial \alpha_c}{}_c\right)}{\alpha_f - \alpha_c}$$

Differentials of α_f, τ_f and τ_c

Gathering coherent error terms and then taking the quadratic average of incoherent terms yields the rms error expressions for α_f;

$$\Delta\alpha_f = \frac{\partial \alpha_f}{\partial \alpha'} k_1 \frac{\Delta \tau_a}{\tau_a} + \frac{\partial \alpha_f}{\partial \alpha} k_2 \frac{\Delta \tau_a}{\tau_a} + \frac{\partial \alpha_f}{\partial a} \Delta a + \frac{\partial \alpha_f}{\partial b} \Delta b + \frac{\partial \alpha_f}{\partial c} \Delta c + \frac{\partial \alpha_f}{\partial \alpha'_c} \Delta \alpha'_c + \frac{\partial \alpha_f}{\partial \alpha_c} \Delta \alpha_c$$

$$\Delta\alpha_f{}^2 = \left(k_1 \frac{\partial \alpha_f}{\partial \alpha'} + k_2 \frac{\partial \alpha_f}{\partial \alpha}\right)^2 \left(\frac{\Delta \tau_a}{\tau_a}\right)^2 + \left(\frac{\partial \alpha_f}{\partial a} \Delta a\right)^2 + \left(\frac{\partial \alpha_f}{\partial b} \Delta b\right)^2 + \left(\frac{\partial \alpha_f}{\partial c} \Delta c\right)^2$$

$$+ \left(\frac{\partial \alpha_f}{\partial \alpha'_c} \Delta \alpha'_c\right)^2 + \left(\frac{\partial \alpha_f}{\partial \alpha_c} \Delta \alpha_c\right)^2$$

Given that $\tau_f = \eta\ \tau_a$ we can express the τ_f and τ_c differentials and their incoherent quadrature sum as below.

$$\frac{d\tau_f}{\tau_a} = \eta\frac{d\tau_a}{\tau_a} + d\eta \text{ and } \frac{d\tau_c}{\tau_a} = \frac{d\tau_a}{\tau_a} - \frac{d\tau_f}{\tau_a}$$

$$\frac{d\tau_f}{\tau_a} = \eta\frac{d\tau_a}{\tau_a} + \left(\frac{\partial\eta}{\partial\alpha'}\Delta\alpha' + \frac{\partial\eta}{\partial\alpha}\Delta\alpha + \frac{\partial\eta}{\partial a}\Delta a + \frac{\partial\eta}{\partial b}\Delta b + \frac{\partial\eta}{\partial c}\Delta c + \frac{\partial\eta}{\partial\alpha'_c}\Delta\alpha'_c + \frac{\partial\eta}{\partial\alpha_c}\Delta\alpha_c\right)$$

$$= \eta\frac{d\tau_a}{\tau_a} + \left(\frac{\partial\eta}{\partial\alpha'}k_1\frac{d\tau_a}{\tau_a} + \frac{\partial\eta}{\partial\alpha}k_2\frac{d\tau_a}{\tau_a} + \frac{\partial\eta}{\partial a}\Delta a + \frac{\partial\eta}{\partial b}\Delta b + \frac{\partial\eta}{\partial c}\Delta c + \frac{\partial\eta}{\partial\alpha'_c}\Delta\alpha'_c + \frac{\partial\eta}{\partial\alpha_c}\Delta\alpha_c\right)$$

$$\left(\frac{\Delta\tau_f}{\tau_a}\right)^2 = \left(k_1\frac{\partial\eta}{\partial\alpha'} + k_2\frac{\partial\eta}{\partial\alpha} + \eta\right)^2\left(\frac{\Delta\tau_a}{\tau_a}\right)^2 + \left(\frac{\partial\eta}{\partial a}\Delta a\right)^2 + \left(\frac{\partial\eta}{\partial b}\Delta b\right)^2 + \left(\frac{\partial\eta}{\partial c}\Delta c\right)^2 + \left(\frac{\partial\eta}{\partial\alpha'_c}\Delta\alpha'_c\right)^2 + \left(\frac{\partial\eta}{\partial\alpha_c}\Delta\alpha_c\right)^2$$

$$\frac{d\tau_c}{\tau_a} = \frac{d\tau_a}{\tau_a} - \eta\frac{d\tau_a}{\tau_a} - \left(\frac{\partial\eta}{\partial\alpha'}k_1\frac{d\tau_a}{\tau_a} + \frac{\partial\eta}{\partial\alpha}k_2\frac{d\tau_a}{\tau_a} + \frac{\partial\eta}{\partial a}\Delta a + \frac{\partial\eta}{\partial b}\Delta b + \frac{\partial\eta}{\partial c}\Delta c + \frac{\partial\eta}{\partial\alpha'_c}\Delta\alpha'_c + \frac{\partial\eta}{\partial\alpha_c}\Delta\alpha_c\right)$$

$$\left(\frac{\Delta\tau_c}{\tau_a}\right)^2 = \left(1 - k_1\frac{\partial\eta}{\partial\alpha'} - k_2\frac{\partial\eta}{\partial\alpha} - \eta\right)^2\left(\frac{\Delta\tau_a}{\tau_a}\right)^2 + \left(\frac{\partial\eta}{\partial a}\Delta a\right)^2 + \left(\frac{\partial\eta}{\partial b}\Delta b\right)^2 + \left(\frac{\partial\eta}{\partial c}\Delta c\right)^2 + \left(\frac{\partial\eta}{\partial\alpha'_c}\Delta\alpha'_c\right)^2 + \left(\frac{\partial\eta}{\partial\alpha_c}\Delta\alpha_c\right)^2$$

$$= \left(\frac{\Delta\tau_f}{\tau_a}\right)^2 + \left(\frac{\Delta\tau_a}{\tau_a}\right)^2\left(1 - 2(k_1\frac{\partial\eta}{\partial\alpha'} - k_2\frac{\partial\eta}{\partial\alpha} - \eta)\right)$$

References

Dubovik, O., B.N.Holben,T. Lapyonok, A.Sinyuk, M. I. Mishchenko, P. Yang, and I.Slutsker, Non-spherical aerosol retrieval method employing light scattering by spheriods,*Geophys. Res. Lett.,* **29**, 54-1 - 54-4, 2002.

Dubovik O., M. D. King, A flexible inversion algorithm for retrieval of aerosol optical properties from Sun and sky radiance measurements, *J. Geophys. Res.*, 105, 20673-20696, 2000.

Eck, T.F., B.N.Holben, J.S.Reid, O.Dubovik, A.Smirnov, N.T.O'Neill, I.Slutsker, and S.Kinne, 1999: Wavelength dependence of the optical depth of biomass burning, urban and desert dust aerosols, J. Geophys. Res., 104, 31 333-31 350.

O'Neill, N. T. , Eck, T. F. , Holben, B. N. , Smirnov, A. , Dubovik, O. ,A. Royer, Bi-modal size distribution influences on the variation of Angstrom derivatives in spectral and optical depth space, J. Geophys. Res., vol. 106, 9787-9806, 2001a.

O'Neill, N. T., Dubovik, O., Eck, T. F., A modified Angstrom coefficient for the characterization of sub-micron aerosols, *App. Opt.*, Vol. 40, No. 15, pp. 2368-2374, 2001b.

O'Neill, N. T.,T. F., Eck, A. Smirnov, B. N.Holben, S. Thulasiraman, Spectral discrimination of coarse and fine mode optical depth, Vol.. 108, *J. Geophys. Res.*, No. D17, 4559-4573, 10.1029/2002JD002975, 2003.

Reid, J. S., S. Piketh, B. N. Holben, D. L. Westphal, A. Al Mangoosh, A. Al Mandoos , R. Bruintjes, A Forward to the United Arab Emirates Unified Aerosol Experiment: UAE^2, submitted to *J. Geophys. Res.*, 2007.

O'Neill, N. T., T.F. Eck, Reid, J. S, Smirnov, A., O. Pancrati, Coarse mode optical information retrievable using ultraviolet to shortwave infrared sunphotometry; application to UAE2, accepted for publication, *J. Geophys. Res.*, 2008a.

O'Neill, N. T., O. Pancrati, K. Baibakov, E. Eloranta, R. L. Batchelor, J. Freemantle, L. J. B. McArthur, K. Strong, R. Lindenmaier, Occurrence of weak, sub-micron, tropospheric aerosol events at high Arctic latitudes, submitted to *Geophys. Res. Lett.*, 2008b